Validation of Rigid-plastic Model for Skeletal Structures under Blast Loading

Final Year Project UG 2017

By

Muhammad Ali Malik

Umer Zeeshan Ibraheem

Shaharyar Atique

Hamza Abaid

Supervisor

Dr. Azam Khan

NUST Institute of Civil Engineering

School of Civil and Environmental Engineering

National University of Sciences and Technology, Islamabad

Pakistan

2021

This is to clarify that the Final Year Project titled

Validation of Rigid-plastic Model for Skeletal Structures under Blast Loading

Submitted By

Muhammad Ali Malik	00000 216607
Umer Zeeshan Ibraheem	00000 226881
Shaharyar Atique	00000 211059
Hamza Abaid	00000 209505

has been accepted towards the requirements for
the undergraduate degree
in
CIVIL ENGINEERING

NUST Institute of Civil Engineering
School of Civil and Environmental Engineering
National University of Sciences and Technology, Islamabad
Pakistan

2021

Acknowledgements

In the name of Allah, the Most Beneficent, the Most Merciful. Peace and blessings be upon our master Muhammad, the servant of Allah and the last of His Final Messenger. First and foremost, all praise and thanks are due to Allah who brought us this far on the path of knowledge and enabled us to conduct this research under competent and accomplished guides and without whose blessing we would not have been able to accomplish such an enormous task. We hope that this work contributes to the development of mankind.

Our parents and mentors have made efforts and sacrifices over the course of our lives to lead us where we stand today for which they have our eternal gratitude. We respect and highly appreciate the guidance and aid provided by our supervisor Dr. Azam Khan, Assistant Professor at NUST Institute of Civil Engineering (NICE) at every step of the way. His valuable advice and calm commitment to this research were a source of motivation for us. Throughout the research project his constant support and taking time out of his busy schedule for mentorship kept us proceeding forward. His professional grooming of the group in thesis writing, presentation and mentorship is a valuable precedent for us that will help us in our practical life.

Special thanks to 3DS for providing us the student licenses of ABAQUS. Finally, we would extend our appreciation towards our friends and colleagues who kept encouraging us and provided necessary assistance in completion of this research project.

Dedication To

Our Supervisor *Dr. Azam Khan*

&

Our families

Table of Contents

ABSTRACT **6**

1. INTRODUCTION **7**
1.1. LITERATURE REVIEW 10

2. PROPOSED DYNAMIC RIGID-PLASTIC MODEL **10**
2.1. REPRESENTATION OF KINETICS AND KINEMATICS AS A NODAL DESCRIPTION 11
2.2. MATERIAL MODEL 14
2.3. THE MATHEMATICAL FORMULATION 17
2.4. INITIATION 19
2.5. PLASTIC UN-STRESSING 22

3. CASE STUDY: TRIANGULAR PRESSURE PULSE ON A SIMPLY SUPPORTED BEAM **22**
3.1. PROBLEM STATEMENT 23
3.2. THEORETICAL RESPONSE OF THE BEAM 24
3.2.1. Phase 1 of motion 24
3.2.2. Phase 2 of motion 27
3.2.3. Static admissibility 28
3.3. LCP PREDICTION OF BEAM RESPONSE 29
3.4. THEORETICAL RESPONSE OF THE BEAM 33
3.4.1. Phase 0 of motion 33
3.4.2. Phase 1 of motion 36
3.4.3. Phase 2 of motion 39
3.5. LCP PREDICTION OF THE BEAM RESPONSE 43

4. CASE STUDY: TRIANGULAR PRESSURE PULSE ON A SINGLE STOREY FIXED ENDED PORTAL FRAME **48**
4.1. PROBLEM STATEMENT 48
4.2. RESPONSE OF THE FRAME PREDICTED BY LCP SOLUTION 49
4.3. RESPONSE OF THE FRAME PREDICTED BY ABAQUS 52

5. CASE STUDY: COMPARISON OF LCP PREDICTION WITH EXPERIMENTAL RESULTS OF REINFORCED CONCRETE BEAM **54**
5.1. EXPERIMENTAL PROGRAM OF ZHANG 54
5.2. RESPONSE OF THE RC BEAM PREDICTED BY LCP SOLUTION 56

6. FINAL COMMENTS **57**

7. REFERENCES **60**

Abstract

This paper proposes a simplified rigid-plastic model for determining the dynamic response of skeletal structures under blast loading. The proposed numerical formalism is an extension of the previously developed model of Khan A et al [1] to investigate the impact behaviour, which is validated for studying the effects of blast loading on skeletal structures. For this purpose, three verification examples are studied. In the first example, a generic theoretical solution is sought for a simply supported beam excited by a uniformly distributed linearly decaying triangular pulse load of varying magnitudes. The numerical and theoretical results are presented and contrasted. In the second study, the dynamic response of a single-story steel portal frame is investigated when the blast load is applied to one of the leg members. This time the result of the proposed model is validated by comparing the maximum deflection with the finite element model developed in ABAQUS. The final validation is made by comparing the experimental results of permanent transverse deformation of blast loaded reinforced concrete beams with the proposed model. The results show that the prediction of the current model is in satisfactory agreement with the experimental results obtained from the literature.

Keywords: Mathematical programming, rigid-plastic model, blast loading, pulse load, beams, frames

1. Introduction

Blast loading response is a large, active, and ever-growing field of studies that encompasses a rich variety of engineering problems, as exemplified by civilian and military structures subject to accidental explosions and terrorist attacks. Such explosions may occur during storage or transport of dangerous substances, such as oil, gas, and radioactive material, as well as ordinary substances, such as milk powder and flour. The ability to predict the response of engineering structures under these loadings is essential for appraising the safety of chemical, nuclear and other manufacturing plants with respect to the potential damage of structural components [2,3]. However, due to the inherent complexity of the blast phenomena and costly experimental setup [4, 5-14], limited analytical and experimental studies can be found in blast load literature. The existing analytical models not only require a high level of expertise but also are computationally expensive and time-consuming [15]. Consequently, rigid-plastic approximations offer a simplified and computationally efficient procedure for dynamic analysis, owing to the exclusion of the elastic response [16]. This simple theory can supply a conceptual framework from which extensions to include the effects of other important parameters can be developed as needed [17].

Although the application of the rigid-plastic theory to dynamic problems was suggested by Taylor [18], the first systematic study in this context appears to have been made by Lee and Symonds [19]. This yielded vast literature on the investigations of structures submitted to extreme dynamic loading [20–29]. Yet it is noteworthy that each closed-form theoretical solution requires to postulate a kinematically admissible velocity profile for the evolution of displaced configuration. Nevertheless, the majority of procedures incorporating the simple rigid-plastic theory are oriented

towards the obtaining of specific results for specific problems, and demand personal judgement for obtaining the best results.

From this precedent, mathematical programming provides an approach to incorporate the rigid plastic theory into a unified formalism that is not specific and problem-oriented. It has a potential to proffer a finite element based numerical formulation [30,31] allowing for a general layout of the structural system with any interconnection between its constituent elements, and the discrete mathematical modelling of the system facilitates the consideration of any distribution of mass, and spatial placement of applied loading and any temporal variation of the associated load pulses [32-35]. Moreover, once the physical modelling decisions have been taken, a complete algorithmic or completely automatic solution procedure can be obtained [36-38].

Mathematical programming [39–42] has a wider application in various specialized fields of engineering, such as robotics [43], fluid simulation [44], and agriculture [45]. The benefits of mathematical programming have been recognized for more than sixty years. Extensive surveys of the use of the mathematical programming application in engineering plasticity have been reported by Maier [30], Maier and Munro [46] and Maier and Lloyd Smith [47, 32].

An important and fundamental development in the theory of the dynamic response of rigid, perfectly plastic continua was offered by the kinematic minimum principle of Tamuzh [48]. Later Capurso [49] used this principle to formulate a mathematical programming problem capable of tracing the response of rigid-plastic framed structures submitted to short duration pulse loads. In recent times, Patsios and Spiliopoulos [50] have analyzed structural frames using the mathematical

programming method. Moreover, Milani and Tralli [51] have employed mathematical programming to model the behaviour of masonry walls. In the context of dynamic problems, the reported applications have been few, but they show promising results [1,52]. Although full of potential, this tool has not been exploited to any great extent to encode and solve problems in dynamic plasticity (Gesualdo et al. 2019).

In a companion paper by Khan et al. [1], a mathematical programming formulation, called the Linear Complementarity Problem LCP [53-58], for determining the response to the rigid-plastic structure was developed. In that study, the LCP solution was employed as a novel simplified design procedure for the assessment of structures under impact loading. The lack of a simple method, for the numerical investigation of skeletal structures subject to explosive loads, has motivated the current investigation to extends this LCP approach for the pulse loaded structures without considering the shear effects. Although the LCP formulation incorporates the philosophy adopted in [1], the physics of blast loading entails an intrinsically different phenomenon than impact problems. The current study proceeds with providing three verification examples testing the accuracy and efficiency of the LCP formulation. First, a theoretical study is undertaken to examine the behaviour of a rigid perfectly plastic beam subjected to varying proportions of triangular pulse-type loading. The beam considered is simply supported at both ends and the blast load is uniformly distributed over the whole span. The LCP execution is validated by comparing various response parameters related to different patterns of motion with the theoretical results. Following this, a second investigation is undertaken into the dynamic plastic response of a rigid-plastic portal frame submitted to blast loading. The LCP predictions are then compared with the

finite element program ABAQUS. Finally, an LCP and experimental investigation of Zhang et al [4] into the dynamic response of fully clamped RCC beam is reported. All these examples are carefully chosen because of their wider use in engineering practice and nevertheless the capability of demonstrating the accuracy and efficiency of the LCP formulation.

1.1. Literature Review

"An Overview of Methods for Blast Load Testing and Devices for Pressure Measurement" written by H. Draganić, D. Varevac, S. Lukić suggested that Experimental tests are limited due to security restrictions and a lack of the considerable resources required and the blast resistance of different types of civilian and military structures against accidental explosions and terrorist attacks is an important security issue. "Behavior of reinforced concrete beams and columns subjected to blast loading" written by Yan Liu, Jun-bo Yan, Feng-lei Huang suggested that the concrete properties must be defined using a nonlinear model CDP i.e., Concrete Damage Plasticity. "Numerical analysis of a reinforced concrete beam under blast loading" written by Yehya Temsah, Ali Jahami, Jamal Khatib, M Sonebi suggested that two explosives having equal scaled distance produces same overpressure on the RC beam. "Structural Impact (2nd edition)" written by Norman Jones suggested that using rigid Plasticity model for observing structural impact on structural members is an accurate and time saving method and analytical model is prepared based on a rectangular pressure pulse.

2. Proposed Dynamic Rigid-Plastic Model

In the current section, the fundamental vectorial conditions, namely the kinetics, the kinematics, and the material constitution, characterizing the behaviour of rigid, perfectly plastic structural

systems undergoing dynamic disturbances due to blast loading, are combined consistently. The structure is envisaged as an assembly of discrete finite beam elements, such as a discretized beam shown in Fig.1, whose structural mass is either concentrated at the boundaries of the elements or continuously distributed along with the elements. The discrete structural system can undergo plastic deformation at the extremities of the finite elements when subject to short term pulse loading. The proposed model can easily be applied to plane frames with boundary conditions of choice.

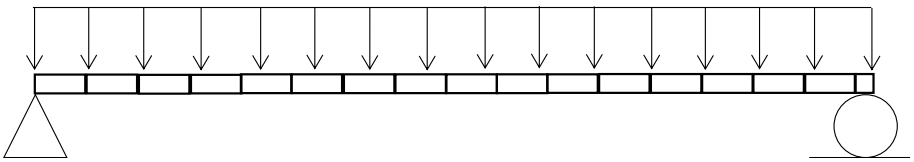

Fig. 1 Discretized simply supported beam under blast loading

2.1. Representation of kinetics and kinematics as a nodal description

The structure in Fig.1 is explored in the nodal description of kinetics and kinematics. Let the structure be subdivided into N finite elements, in which the independent movements of the interconnecting nodes are governed by β degrees of freedom. Any kinematically consistent velocity distribution or profile may be specified completely in terms of β independent nodal velocities $\dot{q}_j \ \ (j = 1,2, \dots \dots, \beta)$. For an assembly of the inextensible planar elements, with α static indeterminacy and S plastic rotational deformations occurring at the element extremities, the kinematic indeterminacy number can be established as $\beta = S - \alpha$.

When each of the β independent nodal velocities $\dot{\mathbf{q}}$ is released, a velocity profile is generated, for which the independent member deformation rates $\dot{x}_h\ (h = 1, 2, \ldots\ldots, 2N)$; indicated in Fig.2, the velocities related to centre of gravity of mass $\dot{u}_k (k = 1, 2, \ldots\ldots, \gamma)$; indicated in Fig.3 and Fig.4, and the load point velocities $\dot{\delta}_\ell\ (\ell = 1, 2, \ldots\ldots, n)$ can be easily obtained through geometric considerations. Hence, the nodal representation of the kinematic equations has the form:

$$\begin{bmatrix} \dot{\mathbf{x}} \\ \dot{\mathbf{u}} \\ \dot{\boldsymbol{\delta}} \end{bmatrix} = \begin{bmatrix} \mathbf{A} \\ \mathbf{A}_d \\ \mathbf{A}_0 \end{bmatrix} \dot{\mathbf{q}} \tag{1}$$

where the coefficient matrix is constant, provided that the motion falls within small displacements.

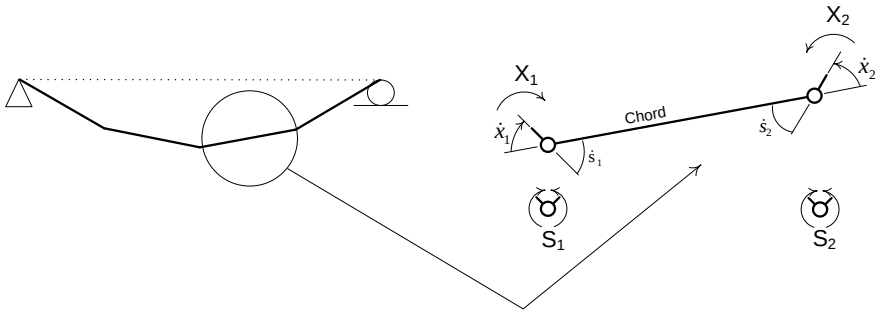

Fig. 2. Stress-resultants, strain-resultant rates, chord deformation rates and independent chord forces

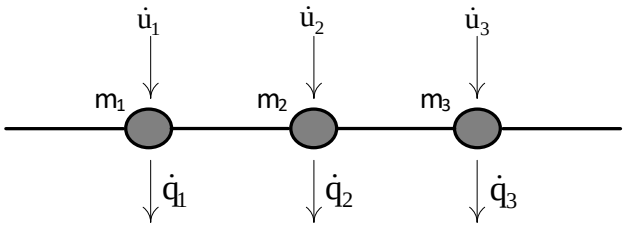

Fig. 3. Centroidal velocities in a lumped mass system

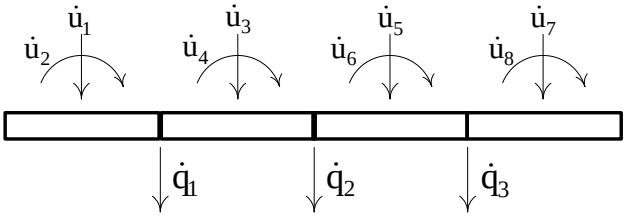

Fig. 4. Centroidal velocities in a continuous mass system

Let the structure be subjected to n discrete time-dependent loads $\lambda_\ell\,(\ell = 1, 2, \ldots\ldots, n)$ applied at the nodes. By employing the D' Alembert principle, during every instant of the accelerated motion of a structure, the applied loads and the inertia forces $\mu_k(k = 1, 2, \ldots\ldots, \gamma)$ are in equilibrium with the independent member forces $X_h\,(h = 1, 2, \ldots\ldots, 2N)$. Corresponding to the independent nodal displacements, the nodal forces of constraint $Q_j(j = 1, 2, \ldots\ldots, \beta)$ are applied. For the satisfaction of the dynamic equilibrium, it is necessary that the constraints Q_j must vanish, giving the nodal kinetics description for the assembly of all elements:

$$\mathbf{Q} = \mathbf{0} = [\mathbf{A}^T \quad \mathbf{A}_d^T \quad \mathbf{A}_0^T] \begin{bmatrix} \mathbf{X} \\ -\boldsymbol{\mu} \\ -\boldsymbol{\lambda} \end{bmatrix} \tag{2}$$

where the transposed (T) coefficient matrix remains constant by the virtue of small displacements. It may be observed that (1) and (2) satisfy the adjoint relationship of kinetic-kinematic duality.

The independent relations (1) and (2) have no cause-effect relationship between the kinetic and kinematic variables. Nevertheless, the relation

$$\boldsymbol{\mu} = -\boldsymbol{m}\,\ddot{\boldsymbol{u}} \tag{3}$$

implicitly links the inertia forces $\mu_k (k = 1, 2, \ldots\ldots, \gamma)$, located at the mass centroid, with the corresponding centroidal accelerations $\ddot{u}_k (k = 1, 2, \ldots\ldots, \gamma)$ of the actual motion of the system. In this inertial law, the diagonal mass matrix $m_k (k = 1, 2, \ldots\ldots, \gamma)$ constitutes the mass or moment of inertia related to the corresponding centroidal accelerations.

2.2. Material Model

The cause-effect relation between the stress-resultant S_1^i (bending moment M_i) and its dual strain-resultant rate $\dot{s}_1^i$ (rotation rate $\dot{\theta}_i$) at critical section i, $(i = 1,2, \ldots, \chi)$, is illustrated in Fig. 5. These quantities are also depicted in the discrete structural model of Fig. 1. It is noted that the plastic moment $X_*^{+i} \geq 0$ when the stress-resultant S_1^i is positive. In Fig 5, it is evident that the yielding at critical section i is defined by two variables, i.e., the plastic potential $y_*^{+i} \geq 0$ and the plastic

multiplier rate $\dot{x}_*^{+i} \geq 0$. A similar argument applies to $X_*^{-i} \geq 0,\ y_*^{-i} \geq 0,\ \dot{x}_*^{-i} \geq 0$ when S_1^i is negative.

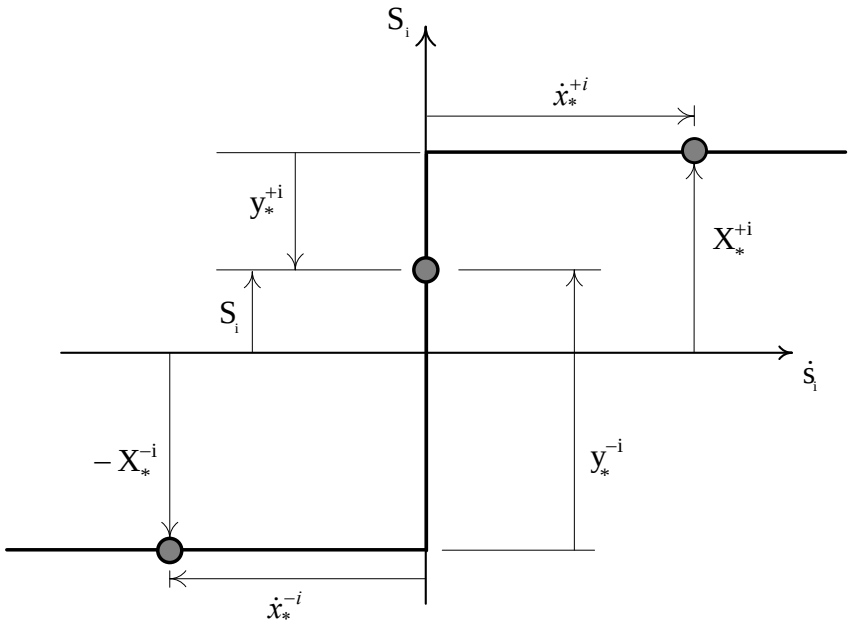

Fig. 5. Variables describing a simple flexural plastic hinge

Now, let the current plastic deformation at the critical section be $s_1^i = x_*^{+i}$ as in Fig. 5. To ensure the irreversible nature of plasticity, it is noted that the plastic deformation $\left(\dot{x}_*^{+i} > 0\right)$, according to a yielding mode may occur only if the corresponding yield limit is attained by the stress $\left(y_*^{+i} = 0\right)$, whereas, if the yield limit is not attained $\left(y_*^{+i} > 0\right)$, then the plastic deformation cannot be active $\left(\dot{x}_*^{+i} = 0\right)$. Mutual exclusivity between each pair of corresponding variables, $\left(\dot{x}_*^{+i} > 0, y_*^{+i} = 0\right)$ and $\left(y_*^{+i} > 0, \dot{x}_*^{+i} = 0\right)$, is assured by the provision of complementarity

condition: $y_*^{+i}\,\dot{x}_*^{+i} = 0$. Now the rigid perfectly plastic constitutive relation for each critical section i is written in matrix notation:

$$\begin{bmatrix} \mathbf{0} & \mathbf{N}^T \\ \mathbf{N} & \mathbf{0} \end{bmatrix} \begin{bmatrix} \dot{\mathbf{x}}_* \\ \mathbf{S} \end{bmatrix} + \begin{bmatrix} \mathbf{y}_* \\ \mathbf{0} \end{bmatrix} = \begin{bmatrix} \mathbf{X}_* \\ \dot{\mathbf{s}} \end{bmatrix} \tag{4}$$

$$\mathbf{y}_* \geq \mathbf{0} \tag{5}$$

$$\mathbf{y}_*^T \dot{\mathbf{x}}_* = 0 \tag{6}$$

$$\dot{\mathbf{x}}_* \geq \mathbf{0} \tag{7}$$

where **N** is the matrix defining the exterior unit normal to the yield function; $N = [\mathbf{I} \quad -\mathbf{I}]$ and $\mathbf{I}$ is the identity matrix.

Relations (4) to (7) represent the nonholonomic constitutive relations of one-dimensional perfect plasticity for the structural system. These relations can be extended for the case where yield is governed by several stress resultants. In such a case the yield surface can be piecewise linearized into a polytope representing the hyperplanes of the polyhedral yield surface [46].

It is of interest to develop a governing mathematical system that couples the constitutive relations, (4) to (7), with the kinetic and the kinematic relations, (1) to (3). Fig.2 clearly illustrates that the independent member forces **X** and the independent member deformation rates $\dot{\mathbf{x}}$ can be defined by the respective stress-resultants **S** and the strain resultant rates $\dot{\mathbf{s}}$. These can be collected for all the constituent finite elements:

$$\dot{\mathbf{x}} = \mathbf{T}\dot{\mathbf{s}}, \tag{8}$$

$$\mathbf{S} = \mathbf{T}^T\mathbf{X} \tag{9}$$

2.3. The Mathematical Formulation

The vectorial relations (1) to (3), together with the triad of complementarity conditions (5) to (7), can be combined into a set of second-order differential equation with respect to time. Nevertheless, this set is made more complex by the complementarity conditions. As no mathematical system is known to this kind of mathematical problem, adopting a numerical solution appears reasonable. Therefore, a time marching scheme is introduced to allow the solution to be advanced from a time station t_n to $t_{n+1} = t_n + \Delta t$, where subscript n is an integer defining successive discrete time stations and Δt in the intervening time increment. Then the centroidal velocities and accelerations can be expressed in Newmark's time-integration scheme:

$$\ddot{\mathbf{u}}_{n+1} = b_0(\dot{\mathbf{u}}_{n+1} - \dot{\mathbf{u}}_n) - b_1\ddot{\mathbf{u}}_n \tag{10}$$

and

$$\dot{\mathbf{u}}_{n+1} = \mathbf{u}_n + b_2\dot{\mathbf{u}}_n + b_3\ddot{\mathbf{u}}_n + b_4\ddot{\mathbf{u}}_{n+1}, \tag{11}$$

in which integration constants are

$$b_0 = \frac{1}{\bar{\gamma}\Delta t}, \tag{12}$$

(13)

$$b_1 = \frac{1-\bar{\gamma}}{\bar{\gamma}},$$

$$b_2 = \Delta t, \tag{14}$$

$$b_3 = (0.5 - \bar{\alpha})\Delta t, \tag{15}$$

$$b_4 = \bar{\alpha}\Delta t^2 \tag{16}$$

It is found after thorough investigations that suitable results are obtained for rigid-plastic dynamics if $\bar{\alpha} = 0.25$ and $\bar{\gamma} = 0.5$.

Collecting (1), (2), (3), and (4) to (7), (8) and (9), at the time $t = t_{n+1}$, and coupling with the Newmark's scheme (10) to (16) the governing system becomes:

$$\begin{bmatrix} -b_0\mathbf{M}_q & \mathbf{0} & -\mathbf{A}^{\mathrm{T}} \\ \mathbf{0} & \mathbf{0} & \mathbf{N}^T\mathbf{T}^T \\ -\mathbf{A} & \mathbf{TN} & \underline{\mathbf{0}} \end{bmatrix} \begin{bmatrix} \dot{\mathbf{q}}_{\mathrm{n+1}} \\ \dot{\mathbf{x}}_{*n+1} \\ \mathbf{X}_{n+1} \end{bmatrix} + \begin{bmatrix} \mathbf{0} \\ \mathbf{y}_{*n+1} \\ \mathbf{0} \end{bmatrix} = \begin{bmatrix} -\mathbf{Y}_{n+1} \\ \mathbf{X}_* \\ \mathbf{0} \end{bmatrix} \tag{17}$$

$$\mathbf{y}_{*n+1} \geq \mathbf{0} \tag{18}$$

$$\mathbf{y}_{*n+1}^T \dot{\mathbf{x}}_{*n+1} = 0 \tag{19}$$

$$\dot{\mathbf{x}}_{*n+1} \geq \mathbf{0} \tag{20}$$

with variables $\dot{\mathbf{q}}_{\mathrm{n+1}}, \mathbf{X}_{n+1}$ unrestricted

The right-hand side sub-vector $\mathbf{Y}_{n+1}$ of (17) is given by:

$$\mathbf{Y}_{n+1} = \mathbf{A}_0^T \boldsymbol{\lambda}_n + \mathbf{M}_q (b_0 \dot{\mathbf{q}}_n + b_1 \ddot{\mathbf{q}}_n), \tag{21}$$

and the mass matrix $\mathbf{M_q}$ is given by the relation:

$$\mathbf{M}_q = \mathbf{A}_d^T \mathbf{m} \mathbf{A}_d \tag{22}$$

The approximating governing system (17) to (20) has a mathematical structure of a linear complementarity problem (LCP). It may be noticed that the variables $\left[\dot{\mathbf{x}}_*, \mathbf{y}_*\right]$ are restrained into the complementary pairs, whereas the leading sub-matrix related to variables[$\dot{\mathbf{q}}$, $\mathbf{X}$] is negative semi-definite. In this work, the governing system is solved efficiently by the Lemke algorithm due to its simplicity and robustness.

2.4. Initiation

The incremental numerical process shown in (17) to (20), representing the evolutive sequence of the dynamic response, is not self-starting. Therefore, it is necessary to establish a subroutine for calculating the relevant accelerations at a certain instant of time. These accelerations are of particular relevance at the commencement of the motion and the deactivation of the previously active section. At such an instant, the vector of plastic multiplier rates $\dot{\mathbf{x}}$ can be separated into Y yielded plastic hinges and R rigid plastic hinges. So, these subsets of the multiplier rates $\dot{\mathbf{x}}$ can be expressed as:

$$Y = \left\{ \left(\dot{\mathbf{x}}_{*y}, \mathbf{y}_{*y} \right) \middle| \dot{\mathbf{x}}_{*y} > \mathbf{0}, \mathbf{y}_{*y} = \mathbf{0} \right\} \tag{23}$$

$$R = \{(\dot{\mathbf{x}}_{*r}, \mathbf{y}_{*r}) | \dot{\mathbf{x}}_{*r} = \mathbf{0}, \mathbf{y}_{*r} \geq \mathbf{0}\} \tag{24}$$

The time-derivative of the discrete law (4) to (7) is formulated as:

$$\begin{bmatrix} \mathbf{0} & \mathbf{0} & \boldsymbol{N}_y^T \\ \mathbf{0} & \mathbf{0} & \boldsymbol{N}_r^T \\ \boldsymbol{N}_y & \boldsymbol{N}_r & \mathbf{0} \end{bmatrix} \begin{bmatrix} \ddot{\boldsymbol{x}}_{*y} \\ \ddot{\boldsymbol{x}}_{*r} \\ \boldsymbol{S} \end{bmatrix} + \begin{bmatrix} \mathbf{0} \\ \boldsymbol{y}_{*r} \\ \mathbf{0} \end{bmatrix} = \begin{bmatrix} \boldsymbol{X}_{*y} \\ \boldsymbol{X}_{*r} \\ \ddot{\boldsymbol{s}} \end{bmatrix} \tag{25}$$

$$\mathbf{y}_{*r} \geq \mathbf{0} \tag{26}$$

$$\mathbf{y}_{*r}^T \ddot{\mathbf{x}}_{*r} = 0 \tag{27}$$

$$\ddot{\mathbf{x}}_{*r} \geq \mathbf{0} \tag{28}$$

$$\ddot{\mathbf{x}}_{*y} \textit{ unrestricted.} \tag{29}$$

It is to Tamuzh [48] that the relation (25) to (29) is due. By comparison of these relations with the nonholonomic laws (4) to (7), it may be seen that the former fail to represent completely the latter in two important cases. Firstly, (29) allows any of the components of $\dot{\mathbf{x}}_{*y}$ to become negative, which would contradict (7). Secondly, these same relations do not allow any of the components of $\dot{\mathbf{x}}_{*r}$ associated with the yield modes, which have become activated during the finite interval, to decrease.

The end of the interval is defined by one or more of the following three criteria:

a) when the relevant functions cease to be differentiable, or

b) when one or more yield modes in set y unstresses, or

c) when one or more yield modes in set r become active.

At the instant so determined, the partition of the sets Y and R must be adjusted and the modified plasticity relations then become valid for a contiguous finite interval of time.

It has been already said that the LCP system (17) to (20) is not self-starting. To initiate this system, regardless of the prescribed displacements $\mathbf{q}_0$ and velocities $\dot{\mathbf{q}}_0$, it is not easy to infer the initial accelerations $\ddot{\mathbf{q}}_0$, and the independent member forces $\mathbf{X}_0$. Differentiating with respect to the time the kinematic relation (1), and together with (25) to (29), Sahlit [37] re-established the governing system in terms of accelerations:

$$\begin{bmatrix} -\mathbf{M}_q & \mathbf{0} & \mathbf{0} & -\mathbf{A}^{\mathrm{T}} \\ \mathbf{0} & \mathbf{0} & \mathbf{0} & \mathbf{N}_{\mathrm{y}}^{\mathrm{T}}\mathbf{T}^{\mathrm{T}} \\ \mathbf{0} & \mathbf{0} & \mathbf{0} & \mathbf{N}_{\mathrm{r}}^{\mathrm{T}}\mathbf{T}^{\mathrm{T}} \\ -\mathbf{A} & \mathbf{T}\mathbf{N}_y & \mathbf{T}\mathbf{N}_r & \underline{\mathbf{0}} \end{bmatrix} \begin{bmatrix} \ddot{\mathbf{q}} \\ \ddot{\mathbf{x}}_{*\mathrm{y}} \\ \ddot{\mathbf{x}}_{*r} \\ \mathbf{X} \end{bmatrix} + \begin{bmatrix} \mathbf{0} \\ \mathbf{0} \\ \mathbf{y}_* \\ \mathbf{0} \end{bmatrix} = \begin{bmatrix} -\mathbf{A}_0^T\lambda_0 \\ \mathbf{X}_{*\mathrm{y}} \\ \mathbf{X}_{*r} \\ \mathbf{0} \end{bmatrix} \tag{30}$$

$$\mathbf{y}_{*r} \geq \mathbf{0} \tag{31}$$

$$\mathbf{y}_{*r}^T\ddot{\mathbf{x}}_{*r} = 0 \tag{32}$$

$$\ddot{\mathbf{x}}_{*r} \geq \mathbf{0} \tag{33}$$

with variables $\ddot{\mathbf{q}}, \ddot{\mathbf{x}}_{*\mathrm{y}}, \mathbf{X}$ unrestricted

If the structure is coerced into motion by an initial impulse or by an initial velocity field, the vector of initial loading is null $\boldsymbol{\lambda}_0 = \mathbf{0}$ at the start of motion. Accordingly, the set of Y active plastic hinges $\left(\dot{\mathbf{x}}_{*\boldsymbol{y}} > \mathbf{0}\right)$ can be easily deduced.

2.5. Plastic Un-stressing

The LCP formulation (17) to (20) only allow the plastic un-stressing at the commencement of each time interval, but not within the increment Δt. This loss of accuracy over a time step leads to spurious oscillations in the stress resultants. Therefore, it is imperative to include a subroutine that calculates the un-stressing time instant $t_{n+\varepsilon}$ within the interval Δt [37]. Thus, the evolutive sequence of the dynamic response is terminated temporarily at the instant when un-stressing is detected. Subsequently, the velocity profile and the partition active Y and in-active R critical sections are adjusted. Once the relevant structural variables at $t_{n+\varepsilon}$ are determined, then, the evolutive process of the LCP system (17) to (20) is re-initiated with $t_{n+\varepsilon}$ as the starting-time.

3. Case Study: Triangular Pressure Pulse on a Simply Supported Beam

The underlying behaviour of a pulse loaded simply supported beam is illustrated in this section. The primary aim is to validate the proposed mathematical model by reference to an exact solution, which has been derived by considering the effects of increasing magnitude of the load pulse. Besides giving insight into the associated physical phenomena, this example is intended to demonstrate the ability and the efficiency of the proposed numerical apparatus to fully represent the mechanics of such structural systems for performing automatic practical response calculations.

3.1. Problem Statement

Let a rigid-perfectly plastic simply supported beam of length $2L$ and uniform mass per unit length m be subjected to a uniformly distributed linearly decaying pulse, shown in Fig. 6. The pulse can be written as:

$$P = P_0\left(1 - \frac{t}{\tau}\right), \qquad 0 \le t \le \tau, \qquad P = 0, \qquad t > \tau \tag{34}$$

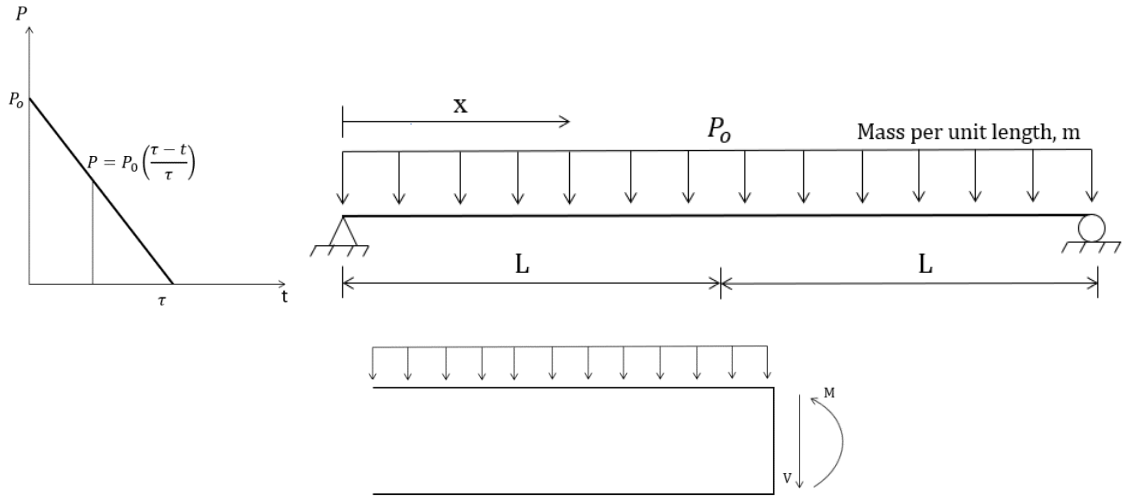

Fig. 6 Simply supported beam subjected to triangular pulse load

Let the fully plastic bending moment of the beam be M_p, while the effect of shear force on yielding be neglected. The exact pressure causing static collapse is given by:

$$P_c = 2\,M_p/L^2 \tag{35}$$

A sequence of the response phases can be performed based on the magnitude of the force P_0. Whenever the applied load is less than the static collapse load P_c, the rigid-perfectly plastic beam remains static and undeformed [3]. The governing equations for the dynamic response of the beam is given by:

$$V = \partial M/\partial x, \tag{36}$$

and:

$$\partial V/\partial x = -P + m\,\partial^2 w/\partial t^2 \tag{37}$$

3.2. Theoretical response of the beam, $P_c \leq P_0 \leq 3P_c$

3.2.1. Phase 1 of motion

An analytical solution is desired using the transverse velocity distribution shown in Fig. 7. The beam is idealized as two rigid arms connected by a stationary plastic hinge located at $x = \xi^*$ from the clamped end. It is found, if $P_c < P_0 < 2P_c$, the motion commences at $t = 0$, and then ceases before the pulse terminates; that is, $t < \tau$. The profile associated with both the rigid arms may be written as:

$$\dot{w} = \frac{x}{L}\dot{W}, \tag{38}$$

for $0 \leq x \leq$ L and $P_c < P_0 \leq 3P_c$,

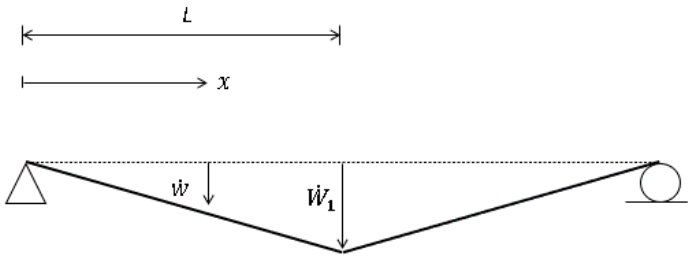

Fig. 7 Distribution of transverse velocity during Phase 1 of the motion

Substituting (34) and (36) in (37) and using the velocity profile (38):

$$\partial^2 M/\partial\, x^2 = -P_0\left(1-\frac{t}{\tau}\right)+m\frac{x}{L}d^2W_1/d\,t^2, \tag{39}$$

Equations (39) may be integrated spatially taking the boundary conditions $M = 0$ at $x = 0$ and satisfying $V = 0$ and at $x = L$.

$$M = P_0\left(1-\frac{t}{\tau}\right)\left(\mathrm{L}x-\frac{x^2}{2}\right)+\frac{m}{2}\frac{d^2W_1}{dt^2}\left(\frac{x^3}{3\mathrm{L}}-\mathrm{L}x\right), \tag{40}$$

for $0 \le x \le L$ and $P_c < P_0 \le 3P_c$,

It is necessary to have $M = M_p$ at $x = L$ in equations (57). Thus,

$$\frac{d^2W}{dt^2} = \frac{3M_p}{mL^2}(\eta\left(\frac{\tau - t}{\tau}\right) - 1), \quad (41)$$

where $\eta = \frac{P_o}{P_c}$

Integrating (41) with time and use $\dot{W}_1 = W_1 = 0\ at\ t = 0$:

$$\frac{dW_1}{dt} = \frac{3M_p}{mL^2}\left(\eta\left(t - \frac{t^2}{2\tau}\right) - t\right) \quad (42)$$

and:

$$W = \frac{3M_p}{mL^2}(\eta\left(\frac{t^2}{2} - \frac{t^3}{6\tau}\right) - \frac{t^2}{2}), \quad (43)$$

As mentioned earlier, if $P_c < P_0 < 2P_c$, the motion ceases before the pulse terminates. The beam will reach its final position when the central velocity $\frac{dW_1}{dt} = 0$, which occurs when:

$$T_f = 2\tau\left(1 - \frac{1}{\eta}\right), \quad (44)$$

However, if $2P_c < P_0 < 3P_c$, the motion continues until $t > \tau$. Therefore, the first phase of motion concludes at $t = \tau$, when the beam has an associated maximum transverse velocity:

$$\dot{W}_1 = \frac{3M_p}{mL^2}\left(\eta\left(\frac{\tau}{2}\right) - \tau\right) \quad ,$$ for $t = \tau$ and $2P_c < P_0 \leq 3P_c$,	(45)

and the peak transverse displacement:

$$W_1 = \frac{3M_p}{mL^2}\left(\eta\left(\frac{\tau^2}{3}\right) - \frac{\tau^2}{2}\right),$$ for $t = \tau$ and $2P_c < P_0 \leq 3P_c$.	(46)

3.2.2. Phase 2 of motion, $2P_c < P_0 < 3P_c$

The beam will be unloaded when the external pressure terminates at $t = \tau$. If the transverse velocity of the beam at time $t = \tau$ conforms to (45), then the beam will continue to deform after time $t \geq \tau$ until the remaining kinetic energy is dissipated at the plastic hinges.

If Phase 2 exists, the velocity distribution described by (38) is supposed to be valid during this phase, except that variables $\dot{w}_1$ & $\dot{W}_1$ are replaced by $\dot{w}_2$ & $\dot{W}_2$ respectively. Similarly, (39) remains unchanged apart from $P_0\left(1 - \frac{t}{\tau}\right) = 0$. Hence (41) becomes:

$$\frac{d^2W_2}{dt^2} = -\frac{3M_p}{mL^2},$$	(47)

for $0 \leq x \leq \xi_*$,	

which may be integrated to give:

$$\dot{W}_2 = \frac{3M_p}{mL^2}(\eta\left(\frac{\tau}{2}\right) - t),$$	(48)

and:

$$W_2 = \frac{3M_p}{mL^2}(\eta\left(\frac{t\tau}{2} - \frac{\tau^2}{6}\right) - \frac{t^2}{2}),$$	(49)

when using (45) and (46) as initial conditions. The motion comes to stand still when $\dot{W}_2 = 0$ according to (48), which occurs when:

$$T_f = \tau\left(\frac{\eta}{2}\right).$$	(50)

3.2.3. Static admissibility

Following the same procedure as [3], it can be easily shown that the theoretical solution presented in the previous subsections do not violate the equilibrium equations (36) and (37), the initial and the boundary conditions. Further, the bending moments satisfy the yield criterion anywhere in the beam for $0 \leq x \leq L$ during both stages of motion. However, yield violation occurs when $P_0 > 3P_c$.

3.3. LCP prediction of beam response, $P_c \leq P_0 \leq 3P_c$

The LCP formulation is tested against the above closed-form solutions. Consider the simply supported beam shown in Fig. 6 that is impelled by a uniformly distributed linearly decaying force pulse. Two amplitudes of pressure pulses are considered, one with force magnitude $P_0 = 1.5P_c$ and non-dimensional duration $\bar{\tau} = M_p\tau/IL = 1.33$, and the other with force magnitude $P_0 = 2.5P_c$ and non-dimensional duration $\bar{\tau} = M_p\tau/IL = 0.8$, where $I = {}^1/_2\, P_0 L$ is the total impulse of the load. The beam is discretized into 100 finite elements with mass lumped at nodes, Fig. 3.

Investigation showed that the LCP offers promising results having small errors in most of the examined quantities. Table 1 presents the results for the non-dimensional central displacement $\bar{W}_1 = (W/L).(mL)M_p/I^2$ and the non-dimensional cessation time $\bar{T}_1 = M_p T_1/IL$, both calculated for the force magnitude $P_0 = 1.5P_c$ and $P_0 = 2.5P_c$**.** It is evident from the table that for $P_c < P_0 < 2.0P_c$ the motion ceases before the pulse terminates at $\bar{\tau} = M_p\tau/IL = 1.33$. Whereas, for $2P_c < P_0 < 3P_c$ the motion continues until after the pulse terminates. Hence, the LCP solution confirms that the dynamic response is characterized by the pulse magnitude.

Table 1: Comparison between theoretical solution and LCP solution at the phase transition

	Theoretical Solution	**Numerical Solution (100 Lumped mass elements)**	**Error (100 Lumped mass elements) (%)**
$\boldsymbol{P_0 = 1.5P_c}$			
Hinge position ξ_*/L	1.0000	1.0000	0.0000
Displacement at the end of motion $\bar{W}_1 = (W_1/L)(mL)M_p/I^2$	0.1975	0.1970	0.3000
Cessation time $\bar{t} = M_pT/IL$	0.8888	0.8960	-0.8000
$\boldsymbol{P_0 = 2.5P_c}$			
Hinge position ξ_*/L	1.0000	1.0000	0.0000
Displacement at the end of the first phase $\bar{W}_1 = (W_1/L)(mL)M_p/I^2$	0.6400	0.6398	0.0200
Displacement at the end of the second phase $\bar{W}_2 = (W_2/L)(mL)M_p/I^2$	0.6999	0.69985	0.0200
Cessation time $\bar{t}_2 = M_pT/IL$	1.0000	0.9999	0.0200

Fig. 8 shows the evolution of non-dimensional central displacement $\bar{W}_1 = (W/L).(mL)M_p/I^2$ at ξ_* (Fig. 7) when $P_0 = 2.5P_c$**.** It is apparent from the figure that the LCP results concur with the theoretical solution.

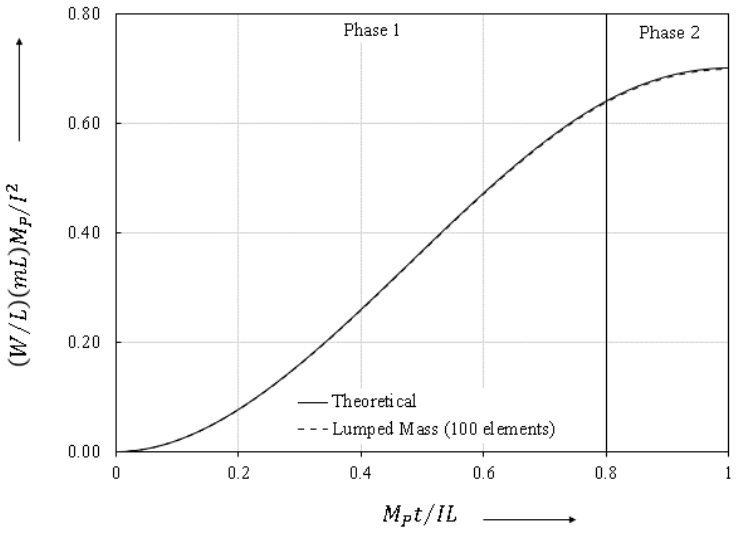

Fig. 8 Evolution of central displacement at ξ_* $(\boldsymbol{P_0 = 2.5P_c})$

Fig. 9 and Fig. 10 show the bending moment distribution across the non-dimensional distance ζ/L from the clamped support of the beam**.** Once again, the accuracy and efficacy of the LCP solution are demonstrated.

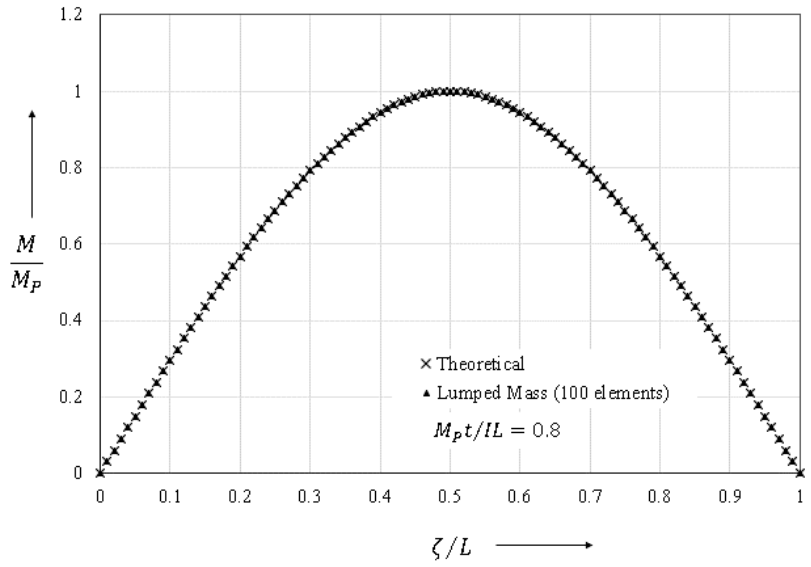

Fig. 9 Dynamic bending moment when the pulse terminates $(P_0 = 2.5P_c)$

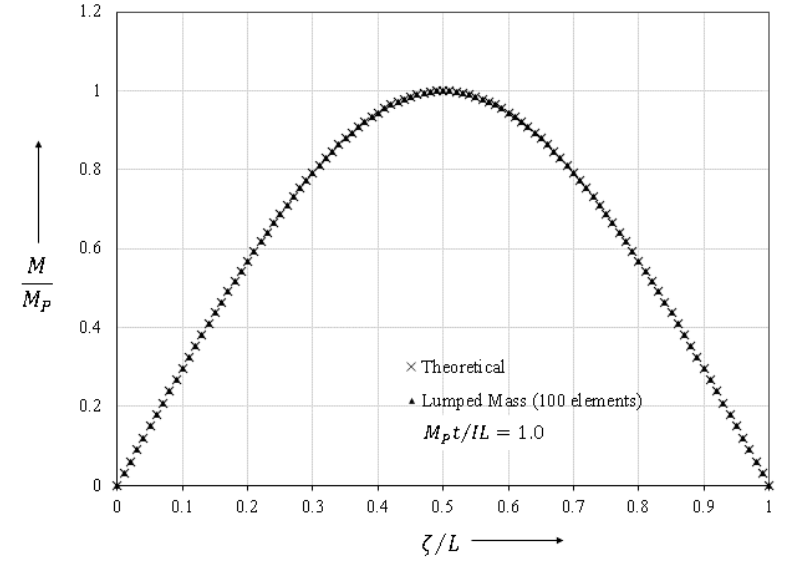

Fig. 10 Dynamic bending moment when the motion ceases $(P_0 = 2.5P_c)$

3.4. Theoretical response of the beam, $P_0 \geq 3P_c$

The theoretical solution presented in Subsection 3.2 is only valid for the pressure pulse $P_c \leq P_0 \leq 3P_c$. Therefore, an alternative transverse velocity field will be sought for pressure pulses with $P_0 \geq 3P_c$. It transpires that for pressure pulses $3P_c < P_0 < 6P_c$ two travelling plastic hinges appear within the beam span and move inward. These hinges coalesce before the pulse terminates. However, if the pressure pulse $P_0 > 6P_c$, then the travelling hinges do not coalesce until after the pulse terminates.

3.4.1. Phase 0 of motion

Initially, at $t = 0$, it is postulated that two plastic hinges form within the beam span. The transverse velocity distribution is in Fig. 11. Thus,

$$\dot{w} = \frac{1}{\xi}\dot{W}_1 x,$$ for $0 \leq x \leq \xi$,	(51)

$$\dot{w} = \dot{W}_1,$$ for $\xi \leq x \leq L$,	(52)

Substituting (34) and (36) in (37), and using the velocity profiles (51) and (52)

$$\partial^2 M/\partial\, x^2 = -P_0\left(1-\frac{t}{\tau}\right) + m\frac{x}{\xi} d^2 W_1/d\, t^2,$$ for $0 \le x \le \xi$,	(53)

and

$$\partial^2 M/\partial\, x^2 = -P_0\left(1-\frac{t}{\tau}\right) + m\, d^2 W_1/d\, t^2,$$ for $\xi \le x \le L$,	(54)

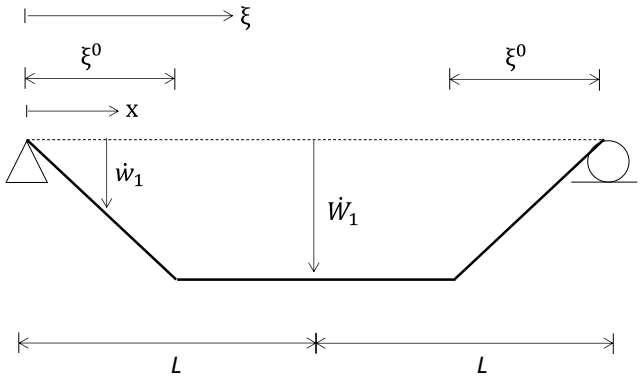

Fig. 11 Distribution of transverse velocity during Phase 1 of motion

It appears reasonable that at $t = 0$ the plastic hinges are assumed stationary at $x = \xi_0$, Fig 11. Equations (53) and (54) may be integrated spatially, taking the boundary conditions $M = 0$ at $x = 0$ and satisfying $V = 0$ and $M = M_p$ at $x = \xi$; therefore,

$$M = -P_o\left(\frac{\tau - t}{\tau}\right)(\xi\, x - \frac{x^2}{2}) + \frac{m}{2\xi}(\frac{x^3}{3} - \xi^{\,2}x).\frac{\partial^2 W_1}{\partial t^2}, \quad (55)$$

for $0 \leq x \leq \xi$,

and:

$$M = M_p, \quad (56)$$

for $\xi \leq x \leq L$.

Integration of (54) with respect to x having the constant of integration evaluated to ensure $V = 0$ at both $x = \xi$ and L yields:

$$\frac{d^2 W_1}{dt^2} = \frac{P_0}{m}\left(1 - \frac{t}{\tau}\right). \quad (57)$$

Equation (53) is identical to (39) but with ξ replaced with L. Thus, the location ξ of the plastic hinge may be found from equating (59) and (57). This gives the value of ξ^0:

$$\xi^0 = \sqrt{\left[6M_p\right]/\left[P_0\left(1 - \frac{t}{\tau}\right)\right]}. \quad (58)$$

Equation (57) may be integrated to give:

$$\frac{dW_1}{dt} = \frac{P_0}{m}\left(t - \frac{t^2}{2\tau}\right),$$	(59)

and:

$$W_1 = \frac{P_0}{m}\left(\frac{t^2}{2} - \frac{t^3}{6\tau}\right),$$	(60)

using initial conditions $\dot{w} = w = 0$ at $t = 0$.

This phase ends at $t > 0$ when the plastic hinge located at ξ start moving.

3.4.2. Phase 1 of motion

During this phase, the plastic hinges at $x = \xi$ (Fig. 11) start travelling towards $x = L$ (Fig. 7). The transverse velocity profile is again assumed to be given by (51) and (52) except that W_1 is replaced by W_2 and the plastic hinges are allowed to move.

Equations (53) and (54) may be integrated spatially taking the boundary conditions $M = 0$ at $x = 0$ and satisfying $V = 0$ and $M = M_p$ at $x = \xi$. Hence,

$$M = -P_o\left(\frac{\tau - t}{\tau}\right)(\xi\, x - \frac{x^2}{2}) + \frac{m}{2\xi}\left(\frac{d^2W_2}{dt^2} - \frac{1}{\xi}\frac{dW_1}{dt}\frac{d\xi}{dt}\right)(\frac{x^3}{3} - \xi^{\,2}x)$$ for $0 \le x \le \xi$,	(61)

and:

$$M = M_p,$$ for $\xi \leq x \leq L$.	(62)

With the aid of (57) and (59), and using the requirement $M = M_p$ at $x = \xi$, equation (61) can be cast in the following form:

$$\frac{d\xi}{dt} = 3M_p \Big/ \left[\xi\, P_0 \left(t - \frac{t^2}{2\tau}\right)\right] - \xi\, \left(1 - \frac{t}{\tau}\right) \Big/ \left[2\left(t - \frac{t^2}{2\tau}\right)\right]$$ for $\xi \leq x \leq$ L.	(63)

It is found that for pressure pulses $3P_c < P_0 < 6P_c$ the two travelling plastic hinges coalesce before the pulse terminates. Whereas, if pressure pulse $P_0 > 6P_c$**,** then the travelling hinges coalesce after the pulse terminates at $t = \tau$. In the former case, equations (57), (59), and (60) can be used. Whereas, in the latter case, again (57), (59), and (60) can be used to get the transverse acceleration, velocity and displacement between $0 < t \leq \tau$. For the subsequent interval $\tau \leq t \leq T_1$, when the pressure pulse is removed, the acceleration $d^2W_2/dt^2 = 0$. Integrating acceleration with respect to time yields the velocity:

$$\frac{dW_2}{dt} = \frac{P_0\tau}{2m},$$	(64)

at $\tau \leq t \leq T_1$ and $P_0 > 6P_c$,	

and the transverse displacement:

$$W_2 = \frac{P_0\tau}{2m}t - \frac{P_0\tau^2}{6m},$$ at $\tau \leq t \leq T_1$ and $P_0 > 6P_c$,	(65)

where the constant of integration ensures that (59) and (60) are recovered at $t = \tau$.

For $3P_c < P_0 < 6P_c$**,** the juncture of the travelling plastic hinges may be found as $\xi_* = L$. These hinges coalesce at the interval T_1 which can be found numerically from equation (63).

When $P_0 > 6P_c$, equation (63) may be used to give the location $\xi^{\#}$ of the plastic hinges at time $t = \tau$ when the pressure pulse is removed. The subsequent position of the travelling plastic hinges can be found from the following equations:

$$(\xi)^2 - (\xi^{\#})^2 = \frac{12M_p}{P_0\tau}(t-\tau),$$ For $\xi \leq x \leq$ L and $P_0 > 6P_c$ at time $\tau \leq t \leq T_1$,	(66)

which, with the aid of $d^2W_2/dt^2 = 0$ and (64), are obtained from (61) where the term involving the pressure pulse is not considered.

The differential equation (63) is solved using the Runge-Kutta fourth-order method. A little finesse is required to initiate the numerical solution, since the time t=0 is a singular point at which the travel velocity of both the span hinges is infinite.

This phase of motion will end at time $t = T_1$ when both travelling plastic hinges reach ξ.

3.4.3. Phase 2 of motion

Phase 2 initiates when the travelling plastic hinges meet at $\xi_* = L$ as presented in Fig. 7. Therefore, the remaining kinetic energy is consumed at hinges located at midspan. This phase ends when the beam come to standstill, so the beam kinetic energy is fully dissipated.

If $3P_c < P_0 < 6P_c$, the stationary hinge remains at midspan with the continuing pulse load. In this case, the governing equations (38) to (41) remain valid, with W_1 replaced by W_3. Whereas, the transverse velocity and the displacement can be obtained by integrating (41) with time and the constants of integration are selected to ensure that (47) and (48) are satisfied at $t = T_1$ when the travelling hinges coalesce. Therefore,

$$\frac{dW_3}{dt} = \frac{3M_p}{mL^2}\left(\xi\left(t - \frac{t^2}{2\tau} - T_1 + \frac{T_1^2}{2\tau}\right) - (t - T_1)\right) + \frac{P_o}{m}\left(T_1 - \frac{T_1^2}{2\tau}\right), \quad (67)$$

for $3P_c < P_0 < 6P_c$ when $T_1 \leq t \leq \tau$,

and:

$$W_3 = \frac{3M_p}{mL^2}\left(\eta\left(\frac{t^2}{2} - \frac{t^3}{6\tau} - T_1 t + \frac{T_1^2 t}{2\tau} + \frac{T_1^2}{2} - \frac{T_1^3}{3\tau}\right) - \frac{(t-T_1)^2}{2}\right) + \frac{P_o}{m}\left(T_1 t - \frac{T_1^2 t}{2\tau} - \frac{T_1^2}{2} + \frac{T_1^3}{3\tau}\right), \quad (68)$$

for $3P_c < P_0 < 6P_c$ when $T_1 \leq t \leq \tau$.

However, if $P_0 > 6P_c$, the pulse terminates before the travelling hinges coalesce. So, equation (39) stay the same except $P_0 = 0$. Therefore:

$$M = \frac{m}{2}\frac{d^2 W_1}{dt^2}\left(\frac{x^3}{3\mathrm{L}} - \mathrm{L}x\right), \quad (69)$$

for $0 \leq x \leq \mathrm{L}$,

$3P_c < P_0 < 6P_c$ when $\tau \leq t \leq T_f$ and $P_0 \geq 6P_c$ when $T_1 \leq t \leq T_f$,

Consequently, the transverse acceleration is:

$$\frac{d^2W_3}{dt^2} = -\frac{3M_p}{mL^2}, \tag{70}$$

for $0 \le x \le \xi_*$,

$3P_c < P_0 < 6P_c$ when $\tau \le t \le T_f$ and $P_0 \ge 6P_c$ when $T_1 \le t \le T_f$,

which may be integrated to give:

$$\frac{dW_3}{dt} = \frac{3M_p}{mL^2}\left(\eta\left(\frac{\tau}{2} - T_1 + \frac{T_1^2}{2\tau}\right) - (t - T_1)\right) + \frac{P_o}{m}\left(T_1 - \frac{T_1^2}{2\tau}\right), \tag{71}$$

for $3P_c < P_0 < 6P_c$ when $\tau \le t \le T_f$,

$$W_3 = \frac{3M_p}{mL^2}\left(\eta\left(\frac{t\tau}{2} - T_1 t - \frac{T_1^2 t}{2\tau} + \frac{T_1^2}{2} - \frac{T_1^3}{3\tau} - \frac{\tau^2}{6}\right) - \frac{(t - T_1)^2}{2}\right) + \frac{P_o}{m}\left(T_1 t - \frac{T_1^2 t}{2\tau} - \frac{T_1^2}{2} + \frac{T_1^3}{3\tau}\right), \tag{72}$$

for $3P_c < P_0 < 6P_c$ when $\tau \le t \le T_f$,

$$\frac{dW_3}{dt} = \frac{3M_p}{mL^2}(T_1 - t) + \frac{P_o\tau}{2m}\ , \qquad (73)$$

for $P_0 \geq 6P_c$ when $T_1 \leq t \leq T_f$,

and:

$$W_3 = \frac{3M_p}{mL^2}\left(\left(T_1 t - \frac{T_1^2}{2} - \frac{t^2}{2}\right)\right) + \frac{P_o}{2m}\left(\tau t - \frac{\tau^2}{3}\right), \qquad (74)$$

for $P_0 \geq 6P_c$ when $T_1 \leq t \leq T_f$,

using (64), (65), (67) and (68) as initial conditions. The motion comes to a stand-still when $\dot{W}_3 = 0$, which occurs when:

$$\mathrm{T}_f = \eta\left(\frac{\tau}{2} - T_1 + \frac{T_1^2}{2\tau}\right) + T_1 + \frac{P_o L^2}{3M_p}\left(T_1 - \frac{T_1^2}{2\tau}\right), \qquad (75)$$

for $3P_c < P_0 < 6P_c$,

and:

$$\mathrm{T}_f = T_1 + \frac{P_o L^2}{3M_p}\tau, \qquad (76)$$

for $P_0 \geq 6P_c$.

3.5. LCP prediction of the beam response, $P_0 \geq 3P_c$

For the LCP solution, the beam shown in Fig. 6 was discretized into $n = 100$ finite elements, chosen as lumped mass elements. Again, two amplitudes of pressure pulses are examined, one with force magnitude $P_0 = 3.5P_c$ and non-dimensional duration $\bar{\tau} = M_p\tau/IL = 0.196$, and the other with force magnitude $P_0 = 12.5P_c$ and non-dimensional duration $\bar{\tau} = M_p\tau/IL = 0.0549$.

The LCP solution shows encouraging results with a small error in most of the examined quantities. Table 2 gives results for the non-dimensional central displacement $\bar{W} = (W/L).(mL)M_p/I^2$ and the non-dimensional time $\bar{t} = M_pT/IL$ both calculated at various phase transitions.

Table 2 Comparison between theoretical solution and LCP solution

	Theoretical Solution	Numerical Solution (100 Lumped mass elements)	Error (100 Lumped mass elements) (%)
$\boldsymbol{P_0 = 3.5P_c}$			
Hinge position $\bar{t} = 0$ (Figure 10) ξ^0/L	0.9305	0.9250	-0.5900
Hinge position at the end of Phase 1 ξ_*/L	1.000	1.000	0.0000
Displacement at the end of Phase 1 $\bar{W}_1 = (W_1/L).(mL)M_p/I^2$	0.0857	0.0857	0.0100
The time when hinges coalesce $\bar{t}_1 = M_pT_1/IL$	0.1632	0.1646	-0.8000
Displacement at the end of motion $\bar{W}_3 = (W_3/L).(mL)M_p/I^2$	0.9263	0.9262	0.0200
Cessation time $\bar{t} = M_pT/IL$	1.0000	1.0000	0.0000
$\boldsymbol{P_0 = 12.5P_c}$			
Hinge position $\bar{t} = 0$ (Figure 10) ξ_1^*/L	0.4990	0.5000	-0.2000
Hinge position at the end of Phase 1 ξ_*/L	1.000	1.000	0.0000
Displacement when the pulse terminates $\bar{W}_1 = (W_1/L).(mL)M_p/I^2$	0.21333	0.21333	0.0000
Displacement at the end of Phase 1 $\bar{W}_2 = (W_2/L).(mL)M_p/I^2$	0.5615	0.5612	0.0400
The time when hinges coalesce $\bar{t}_1 = M_pT_1/IL$	0.3333	0.3340	-0.2200
Displacement at the end of motion $\bar{W}_3 = (W_3/L).(mL)M_p/I^2$	1.2270	1.2265	0.01
Cessation time $\bar{t} = M_pT/IL$	1.0000	1.0000	0.0000

Fig. 12 indicates the evolution of the non-dimensional midspan central displacement throughout Phases 1 and 2 of motion for the pulse magnitude $P_0 = 12.5P_c$. It is evident that the LCP results agree substantially with the theoretical solution.

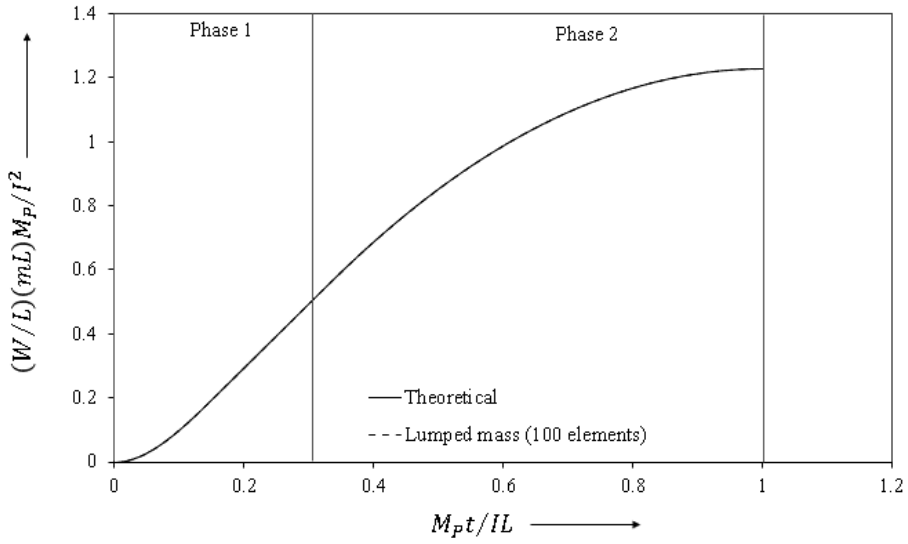

Fig. 12 Central displacement at ξ_* ($\boldsymbol{P_0 = 12.5P_c}$)

At the time of pulse application, two plastic hinges are formed at ξ^0 from both supports, Fig 11. Reference Fig. 13 and Fig. 14 which show the path traced by the travelling plastic hinges for $P_0 = 12.5P_c$. The phase terminates when the travelling hinges reach $\xi/L = 0.5$ at non-dimensional time $\bar{t}_1 = \frac{M_p T_1}{IL} = 0.3340$.

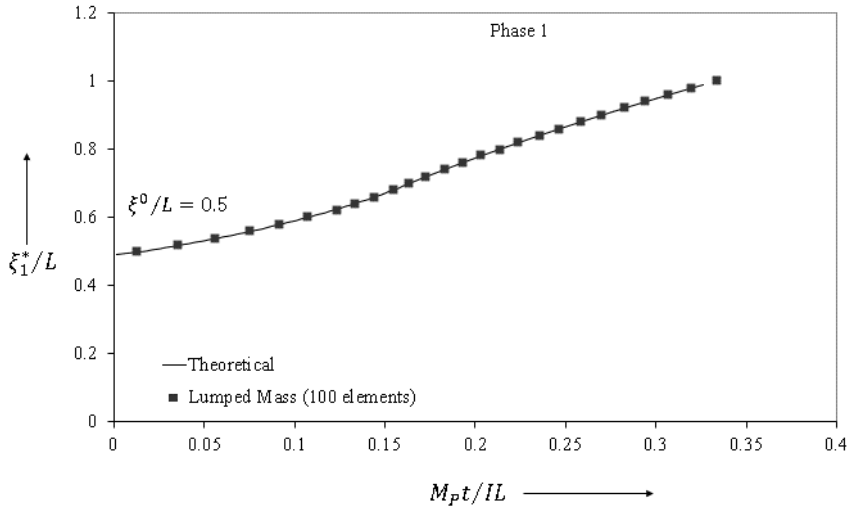

Fig. 13 Movement of plastic hinge away from clamped end ($P_0 = 12.5P_c$)

Fig. 15 indicates the bending moment evolution of the beam at phase transition for both the theoretical and the LCP models. The bending moment distribution is for the decaying pulse with initial amplitude $P_0 = 12.5P_c$. Again, both the LCP solution and the theoretical solution show substantially close agreement from the start until the end.

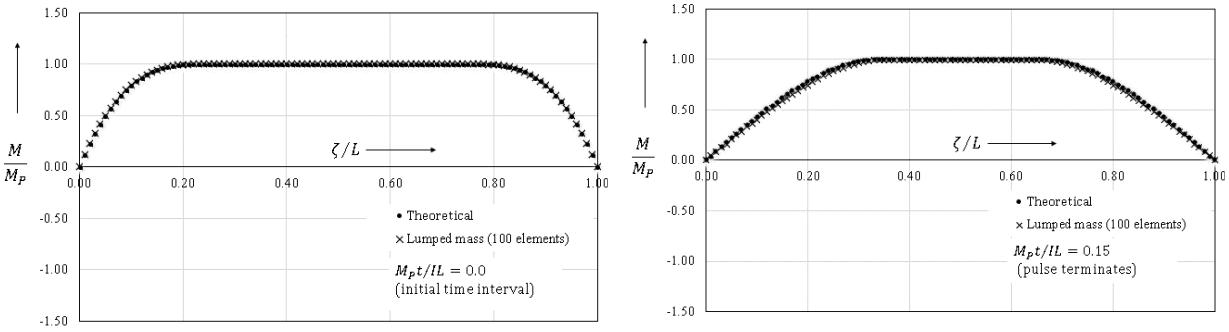

(a) **(b)**

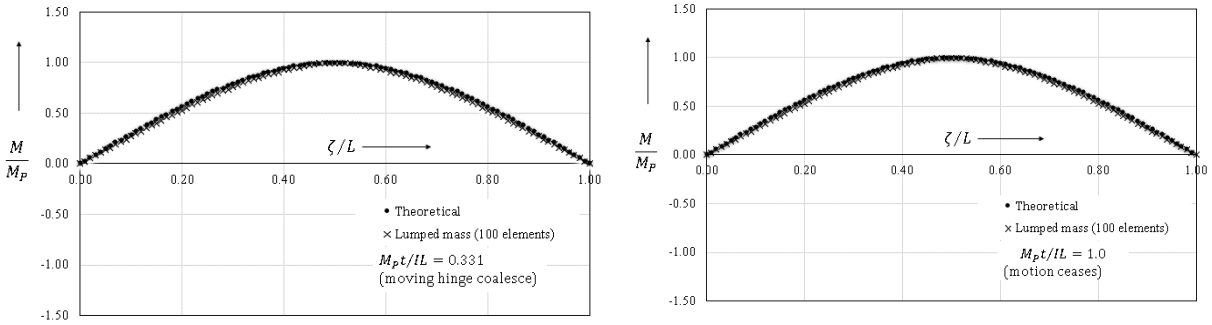

(c) **(d)**

Fig. 14 Dynamic bending moment evolution $(P_0 = 12.5P_c)$

4. Case Study: Triangular Pressure Pulse on a Single Storey Fixed Ended Portal Frame

4.1. Problem statement

As a second example, the dynamic response of a single storey portal frame with fixed bases, as shown in Figure 15, has been calculated for a triangular pulse load of 6.55 N/mm^2 applied for a duration of 0.0082 sec. To relate the discussion to a more practical context, the adopted frame has a 3.5m beam and columns, fabricated from a UKB 610x305x179 section in S355 steel for which the unit mass is 179 kg/m and the plastic moment of resistance is 1910 KNm. The frame is subjected to a uniformly distributed triangular pulse load 2011 N/m applied on the left column as shown in Figure 5

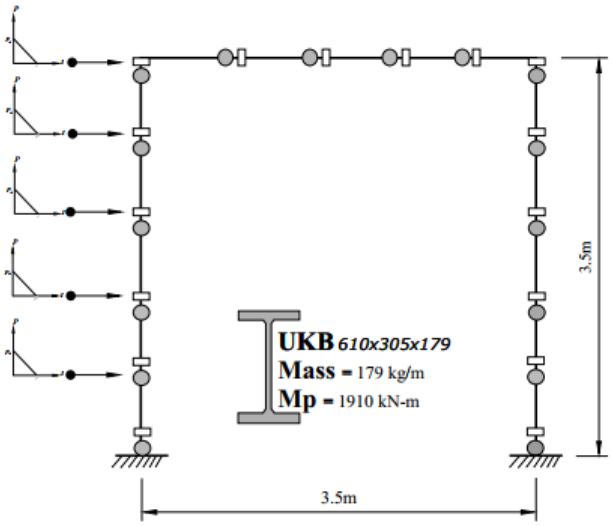

Fig. 15 Portal frame impelled by blast loading

4.2. Response of the frame predicted by LCP solution

The portal frame was sub-divided into 30 contiguous lumped mass elements (5 elements per member) and is exposed to a triangular pulse loading over the left leg of the frame. The potential location of the plastic hinges is shown by a symbol in Figure 16. The ensuing motion, initiated from the profile shown in Figure 17(a), exhibits three distinct phases or mode forms. The first three phases may be regarded as a transient sequence culminating in a final phase. Figure 17 also shows the time of termination of the respective phases, location of activated hinges and the associated drift of frame. It is interesting to note that the motion ceases before the termination of the pulse.

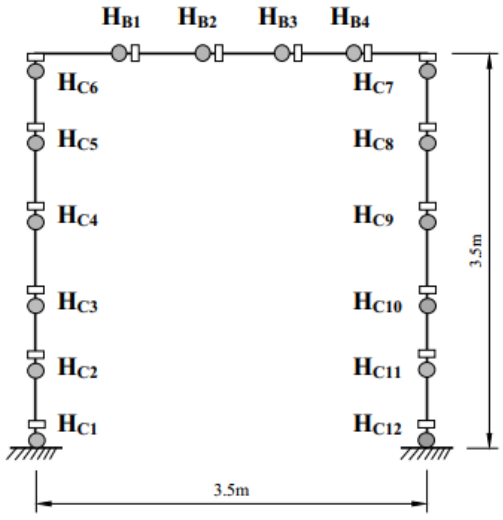

Fig. 16 Lumped Mass Symbols

The evolution of the strain rate of activated hinges and the column bending moments of the frame is presented in Figure 18 and Figure 19 respectively. It is clear that there are always four

sections active during each phase of motion. The bending moment of the activated hinges remain constant within each phase, and the moment may vary when the hinge deactivates. It is important to emphasize that the bending moments given by the LCP are kinetically admissible but not necessarily unique. Finally, it is important to remark that the time step Δt to capture this dynamic response was set at 0.00008 sec.

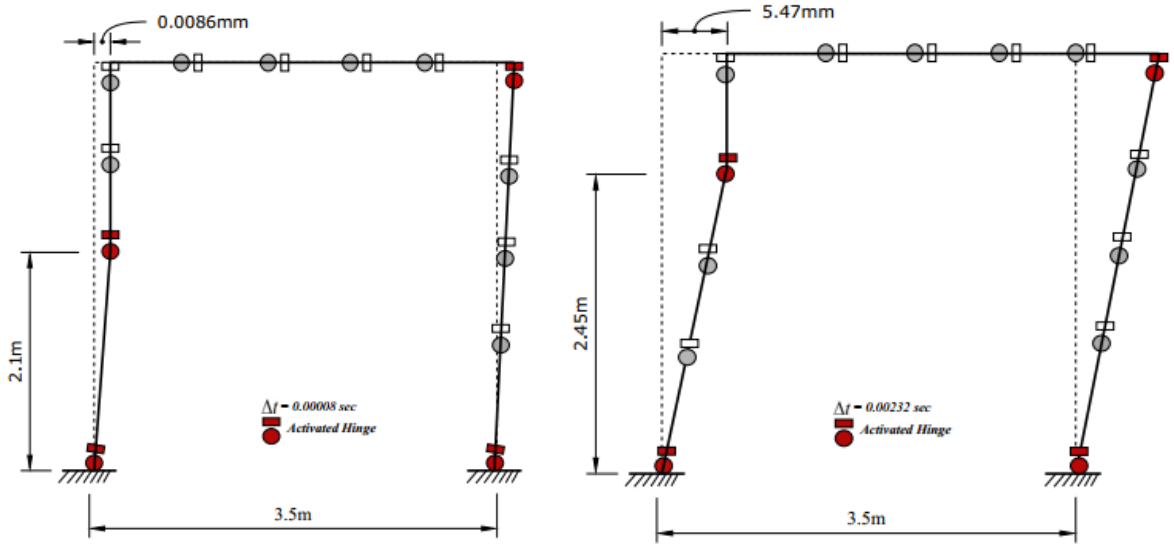

(a) **(b)**

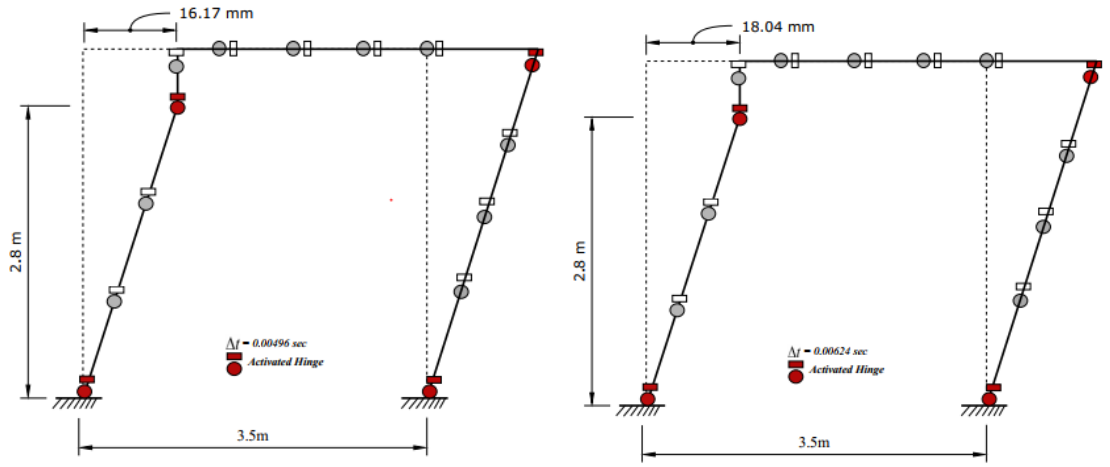

(c) **(d)**

Fig. 17 Evolution of displacement profiles

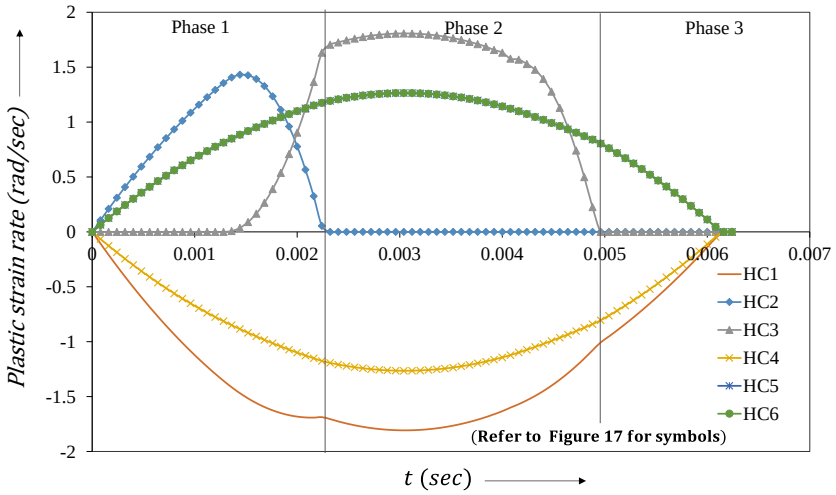

Fig. 18 Evolution of plastic strain rates

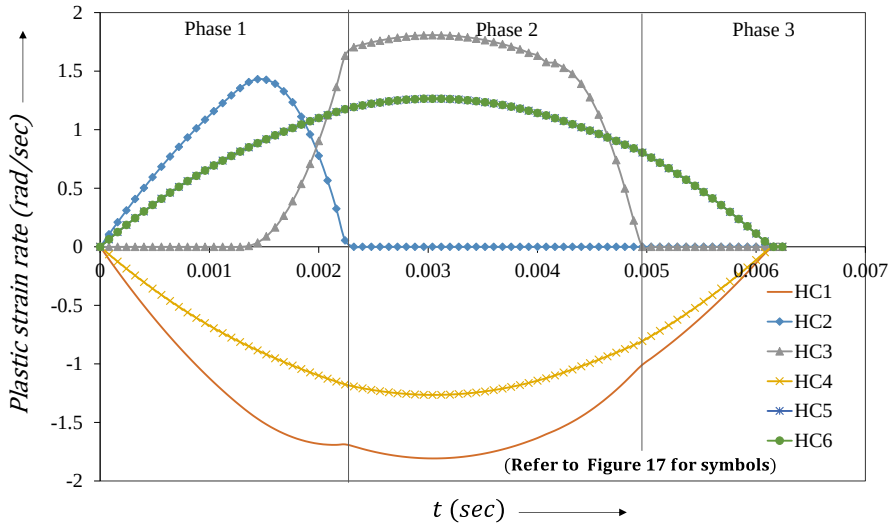

Fig. 19 Evolution of plastic strain rates

4.3. Response of the frame predicted by ABAQUS

The primary aim of this subsection is to validate the frame displacement against the full 3D numerical model in finite element commercial software ABAQUS Explicit. Tetrahedral brick elements are used to model the full length of the frame shown in Figure 16 having clamped boundary condition and subjected to pressure type loading of 6.55 N/mm^2. The frame has prescribed a density of 7850 kg/m^3 , the Poisson's ratio of 0.3 and Young modulus of 91,000 GPa, which is the maximum possible stiffness at which ABAQUS gives sensible results. This strategy of using high magnitude young modulus is considered an appropriate vehicle for the comparison of rigid-plastic LCP results with those of ABAQUS. A convergence study is carried out to optimize the mesh size. The validity of the results is examined by making a comparison between the displacement time histories of the frame obtained from the LCP and ABAQUS approaches, Fig. 20 and Fig. 21. In general, the LCP sway displacement concurs with the results

of ABAQUS. Furthermore, it is observed that the location of plastic hinges in the final phase of motion shown in Fig. 17 coincides with that depicted by Misses stress field in Fig 22

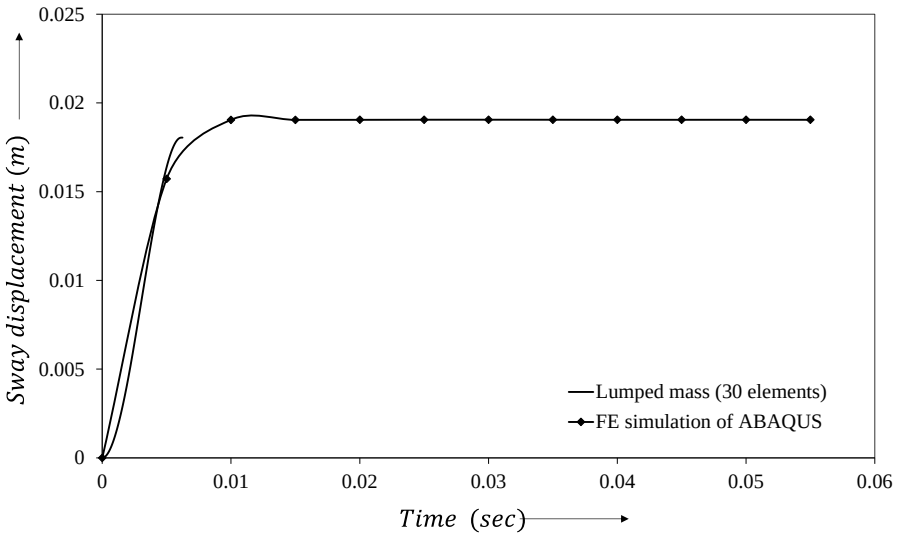

Fig. 20 Maximum displacement time histories of LCP model and ABAQUS

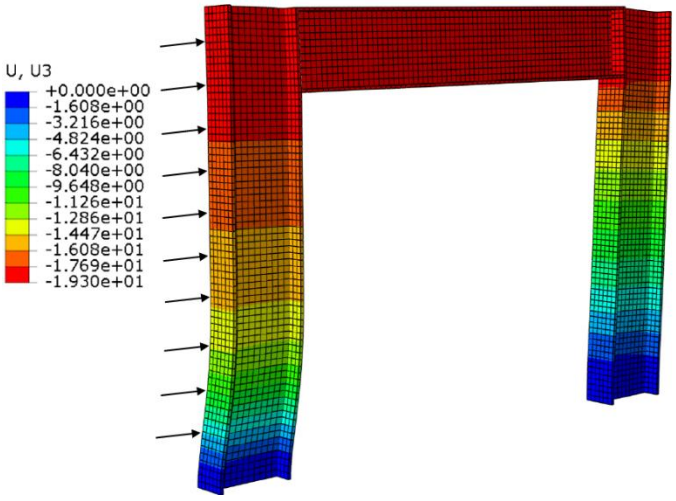

Fig. 21 Maximum sway displacement of ABAQUS frame

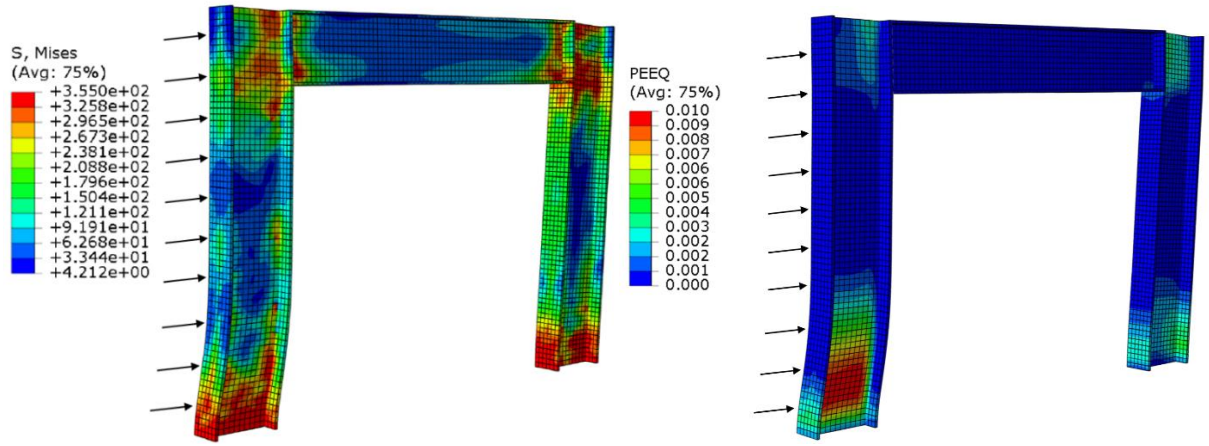

Fig. 22 Final Distribution Mises stress and Equivalent Plastic strain in ABAQUS Frame

5. Case Study: Comparison of LCP prediction with experimental results of reinforced concrete beam

The dynamic response of a clamped reinforced concrete beam subjected to blast loading has been examined experimentally by many researchers. It is aimed in this section to compare the existing experimental results with the predicted results of the LCP. To be specific, particular attention has been focused on the LCP midspan deflection at standstill and the test results are borrowed from the experimental study of Zhang et al [4].

5.1. Experimental Program of Zhang [4]

As part of the Zhang et al [4] experimental program, a series of 1100mm beams were tested under a variable TNT mass and identical standoff distance of 400mm, as shown in Fig 23. The RC beam was of 40Mpa compressive strength having a square cross-section of 100mmx100mm and 20mm cover all around. Further, the longitudinal and transverse bars were of 6mm diameter, with the yield and ultimate strength of 395 Mpa and 501 MPa, and the spacing of stirrups was

60mm. For the current LCP validation of RC beams subjected to blast loading, a companion set of two beams is selected with identical properties but different blast loads of 0.36 kg and 0.45 kg of TNT. Following Zhang's classification of tested specimens, the beam under blast load having an explosive charge weight of 0.36 kg is named B2-1, and the other beam under the charge weight of 0.45 kg is named B2-2, Fig 23.

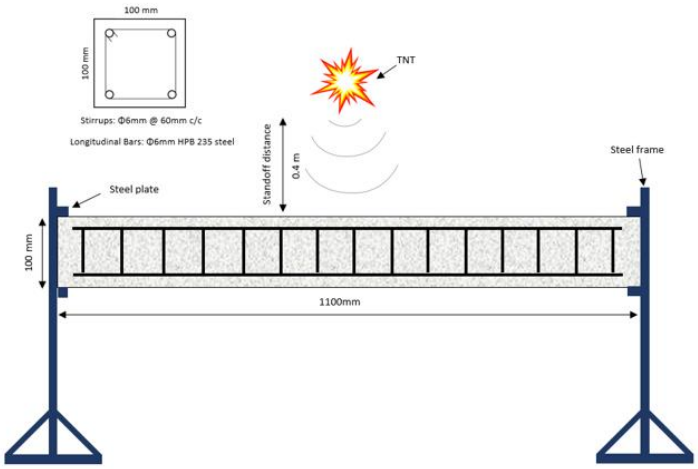

(a)

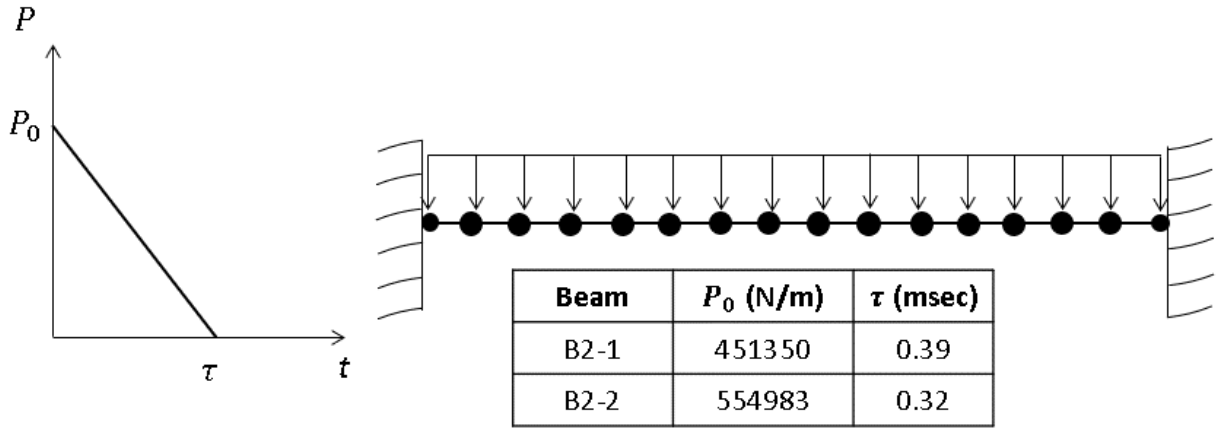

Beam	P_0 (N/m)	τ (msec)
B2-1	451350	0.39
B2-2	554983	0.32

(b)

Fig. 23 RC beam under blast loading: (a) Zhang [4] experimental setup (b) LCP model of RC beam

5.2. Response of the RC beam predicted by LCP solution

The dynamic response of the beams is predicted using a rigid-plasticity based LCP model, Fig 23. The LCP beam is sub-divided into 30 contiguous lumped mass element, which is obtained from the mesh convergence tests of the beam. The beam has a unit mass of 24 kg/m and the plastic moment of resistance is 1710 Nm. Two different blast loading scenarios are investigated for the same pulse duration as shown in Fig 23. Using the scaled distance and charge mass, Newmark [59] formulation is employed for computing peak overpressure value. Fig. 24 shows the comparison of maximum mid-span displacements of the RC beam between those from the LCP and the experimental results. Zhang [4] has reported the maximum deflection value for B2-1 as 9mm and B2-2 as 25mm. Comparing these values to the LCP results of 8.7 mm for B2-1 and 22mm for B2-2, it can be argued that the LCP results are reasonably reliable.

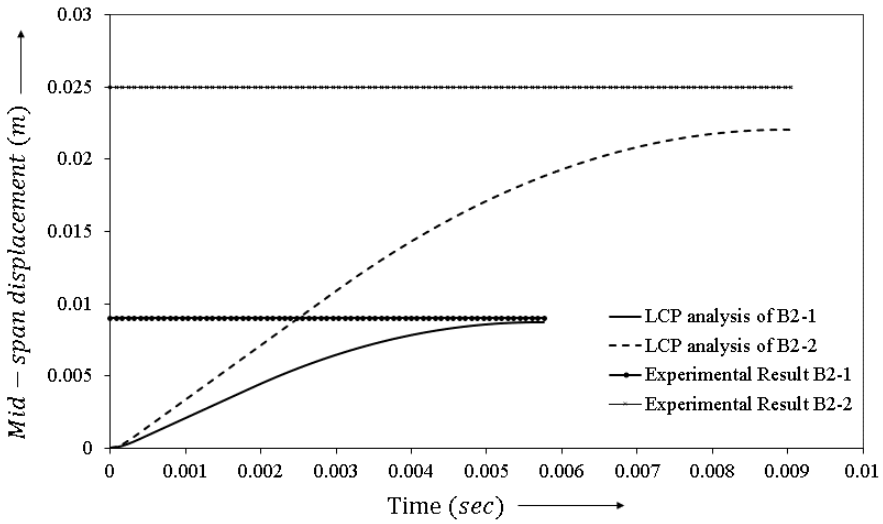

Fig. 24 Comparison of LCP results with experimental results

6. Final Comments

It may be needless to say that the rigid-plastic dynamic analysis is adequately expressive of the true behaviour of the concrete and the steel structures, provided that the total input energy transmitted to the structure is significantly larger than the maximum stored elastic strain energy. By excluding all the elastic deformation, rigid-plastic dynamics allow gaining insights into the precise mechanisms responsible for dissipating the plastic energy. Rigid-plastic theory constitutes an intuitive appreciation of plastic deformation, whereas the elastoplastic theory, although embracing all relevant parameters, tends to define less sharply the evolution of the plastic deformation mechanism.

In the context of establishing a systematic solution procedure for the problems in the rigid-plastic dynamics, a formulation such as a linear complementarity problem (LCP) has been applied with a substantial reward. The LCP formulation is fully automatic and can take full account of any arbitrary pulse shape. It has been shown that the procedure generates the complete evolution of all response parameters.

Three examples are reported to demonstrate the accuracy of the LCP formulation. First, a theoretical study is illustrated to explore the underlying mechanics of a rigid-plastic simply supported beam acted on by a linearly decaying triangular pulse. While giving insight into the associated physical phenomena, this example clearly shows that the proposed LCP model fully represent the actual mechanics of such a structural system and that the corresponding numerical implementations can perform practical response calculations automatically. It is seen that the LCP formulation can produce the full evolution of the whole process of displacement and the plastic deformation, from the initial pulse application to the eventual standstill. With the masses being lumped at the element ends, the LCP solution traced the theoretical solution remarkably well. For instance, the error in the central displacement in the case of 100 lumped mass elements was observed to be less than 1.5% (Tables 1 and 2).

An example of a steel portal frame details the second LCP validation. It is shown that the systematic solution procedure for the LCP enables the travelling plastic hinge movements to be approximated through a sequence of mechanical movements or velocity profiles. Due to the considerable numerical complexity posed by developing a theoretical solution, validation is undertaken by an elastoplastic solution provided by the nonlinear finite element structural analysis

environment, ABAQUS. It transpires that the plastic deformation is difficult to identify in elastic-plastic response because the plastic and elastic deformations are interspersed. Nevertheless, the final deformation mode of the ABAQUS frame model is broadly similar to that of the rigid-plastic model. The investigation of 30 lumped mass elements LCP frame showed less than 1% error in sway displacement compared to ABAQUS tetrahedron brick element frame.

The third validation is to compare the experimental and the LCP mid-span displacement for a blast loaded RC beam with both ends clamped. The experimental results are borrowed from literature for two triangular pules that have a different impulse. The LCP solution for the lumped mass discretization of 50 elements can capture the mid-span deflection satisfactorily.

Finally, it is worth asserting that the rigid-plastic LCP formulation can prove useful during the preliminary design stages of skeletal structures subjected to blast loads. The proposed method is capable of predicting the main features of behaviour for a particular structural design rather quickly. For problems where increased accuracy or further details of the structural behaviour is required, then the present approach may be straightforwardly extended to incorporate additional aspects, such as strain rate, strain hardening and large displacements.

References

[1] Khan A, Smith DL, Izzuddin BA. Investigation of rigid-plastic beams subjected to impact using linear complementarity. Eng Struct 2013;50:137–48.

[2] Chen S, Li Q, Liu Y, Xia J, Xue Z. Dynamic elastoplastic analysis using the meshless local natural neighbour interpolation method. Int J Comput Methods 2011;8:463–81.

[3] Jones N., Structural Impact, Cambridge University Press, 1989

[4] Zhang D., Yao S., Lu F., Chen X., Lin G., Wang W., Lin Y., Experimental Study on scaling of RC beams under close-in blast loading, Engineering Failure Analysis, Vol 33, pp 497-504, 2013

[5] Yan Liu, Jun-bo Yan, Feng-lei Huang, Behavior of reinforced concrete beams and columns subjected to blast loading, Defence Technology, Vol 14

[6] MinJoo Lee and Hyo-Gyoung Kwak, Blast and Impact Analyses of RC Beams Considering Bond-Slip Effect and Loading History of Constituent Materials, International Journal of Concrete Structures and Materials.

[7] Yang Li, Omar Algassem, Hassan Aoude, Response of high-strength reinforced concrete beams under shock-tube induced blast loading, Construction and Building Materials, Vol 189.

[8] Jin-Young Lee, Hyun-Oh Shin, Doo-Yeol Yoo, Young-Soo Yoon, Structural response of steel-fiber-reinforced concrete beams under various loading rates, Engineering Structures, Vol 156.

[9] J. Magnusson, M. Hallgreny and A. Ansell, Air-blast-loaded, high-strength concrete beams, Part I: Experimental investigation, Magazine of Concrete Research 2010.

[10] Yehya Temsah, Ali Jahami, Jamal Khatib, M Sonebi, Numerical analysis of a reinforced concrete beam under blast loading, MATEC Web of Conferences.

[11] Ali Jahami, Yehya Temsah, Jamal Khatib, The efficiency of using CFRP as a strengthening technique for reinforced concrete beams subjected to blast loading, International Journal of Advanced Structural Engineering (2019).

[12] Ann M Biju, Athulya Sreesa E K, Devika Remesh, Rinsa K, Anusree A, Numerical Study of Reinforced Concrete beam subjected to blast loading using Finite element package ABAQUS, IOSR Journal of Mechanical and Civil Engineering (IOSR-JMCE)

[13] J. Magnusson & M. Hallgren, Reinforced high strength concrete beams subjected to air blast loading, Structures Under Shock and Impact VIII.

[14] Yang Li, Omar Algassem, Hassan Aoude, Response of high-strength reinforced concrete beams under shock-tube induced blast loading, Construction and Building Materials, Vol 189.

[15] Jones N. Plastic failure of ductile beams loaded dynamically 1976.

[16] Jones N. Some Comments on the Dynamic Plastic Behaviour of Structures. (Retroactive Coverage). Int. Symp. Intense Dyn. Load. Its Eff., 1986, p. 49–71.

[17] Cennamo C, Gesualdo A, Monaco M. Shear plastic constitutive behaviour for near-fault ground motion. J Eng Mech 2017;143:4017086.

[18] Taylor GI. The use of flat-ended projectiles for determining dynamic yield stress I. Theoretical considerations. Proc R Soc London Ser A Math Phys Sci 1948;194:289–99.

[19] Lee EH, Symonds PS. Large plastic deformations of beams under transverse impact. J Appl Mech ASME 1952;19:308–14.

[20] Bleich HH, Shaw R. Dominance of shear stresses in early stages of impulsive motion of beams 1960.

[21] Jones N, Shen WQ. Criteria for the inelastic rupture of ductile metal beams subjected to large dynamic loads. Struct. crashworthiness Fail., Elsevier London; 1993, p. 95–130.

[22] Ling Q, He Y, He Y, Pang C. Dynamic response of a multibody structure subjected to blast loading. Eur J Mech 2017;64:46–57.

[23] Lowe WT, Al-Hassani STS, Johnson W. Impact behaviour of small scale model motor coaches. Proc Inst Mech Eng 1972;186:409–19.

[24] Mehreganian N, Fallah AS, Louca LA. Plastic dynamic response of simply supported thick

square plates subject to localised blast loading. Int J Impact Eng 2019;126:85–100.

[25] Menkes SB, Opat HJ. Broken beams. Exp Mech 1973;13:480–6.

[26] Parkes EW. The permanent deformation of a cantilever struck transversely at its tip. Proc R Soc London Ser A Math Phys Sci 1955;228:462–76.

[27] Parkes EW. The permanent deformation of an encastré beam struck transversely at any point in its span. Proc Inst Civ Eng 1958;10:277–304.

[28] Symonds PS. Survey of methods of analysis for plastic deformation of structures under dynamic loading. Division of Engineering Report BU/NSRDC/; Brown University: Providence, RI, (1967) 1-148, 1967.

[29] Symonds PS, Frye CWG. On the relation between rigid-plastic and elastic-plastic predictions of response to pulse loading. Int J Impact Eng 1988;7:139–49.

[30] Maier G. Mathematical programming applications to structural mechanics: some introductory thoughts. Eng Struct 1984;6:2–6.

[31] Martin JB. A note on the uniqueness of solutions for dynamically loaded rigid-plastic and rigid-viscoplastic continua 1966.

[32] Smith DL. Plastic limit analysis and synthesis of structures by linear programming. PhD thesis, Department of Civil Engineering, Imperial College, University of London, 1974.

[33] Appleton JADS. Elastoplastic analysis of skeletal structures by mathematical programming.

Imperial College London, 1979.

[34] de Freitas JAT. The elastoplastic analysis of planar frames for large displacements by mathematical programming. PhD thesis, Civil Engineering Department, Imperial College, University of London, 1979.

[35] Al-Samara MA. Elastoplastic dynamics of skeletal structures by mathematical programming. PhD thesis, Department of Civil Engineering, Imperial College, University of London, 1986.

[36] Chuang P-H. Fuzzy mathematical programming in civil engineering systems. PhD thesis, Civil Engineering Department, Imperial College, University of London, 1985.

[37] Sahlit CLDM. Mathematical programming methods for dynamically loaded rigid-plastic framed structures. PhD thesis, Civil Engineering Department, Imperial College, University of London, 1992.

[38] Khan A. Behaviour of rigid plastic structures under extreme dynamic loading. PhD thesis, Civil Engineering Department, Imperial College, University of London, 2009.

[39] Dantzig GB. Linear programming and extensions. vol. 48. Princeton university press; 1998.

[40] Dantzig GB, Orden A, Wolfe P, others. The generalized simplex method for minimizing a linear form under linear inequality restraints. Pacific J Math 1955;5:183–95.

[41] Lemke CE. Some pivot schemes for the linear complementarity problem. Complement.

Fixed Point Probl., Springer; 1978, p. 15–35.

[42] Murty KG. Linear programming. Springer; 1983.

[43] Nuseirat AMA-F, Stavroulakis GE. A complementarity problem formulation of the frictional grasping problem. Comput Methods Appl Mech Eng 2000;190:941–52.

[44] Andersen M, Niebe S, Erleben K. A fast linear complementarity problem solver for fluid animation using high-level algebra interfaces for GPU libraries. Comput Graph 2017;69:36–48.

[45] Garrido A, Antonelli L, Martin J, Alemany MME, Mula J. Using LEL and scenarios to derive mathematical programming models. Application in a fresh tomato packing problem. Comput Electron Agric 2020;170:105242.

[46] Maier G, Munro J. Mathematical programming applications to engineering plastic analysis. Appl Mech Rev 1982;35:1631–43.

[47] Maier G, Smith DL. Update to mathematical programming applications to engineering plastic analysis. Appl Mech Updat 1986:377–83.

[48] Tamuzh VP. On a minimum principle in dynamics of rigid-plastic bodies. J Appl Math Mech 1962;26:1067–77.

[49] Capurso M. A quadratic programming approach to the impulsive loading analysis of rigid plastic structures. Meccanica 1972;7:45–57.

[50] Patsios TN, Spiliopoulos K V. A force-based mathematical programming method for the incremental analysis of 3D frames with non-holonomic hardening plastic hinges. Comput Struct 2018;208:51–74.

[51] Milani G, Lourenço PB, Tralli A. Homogenized rigid-plastic model for masonry walls subjected to impact. Int J Solids Struct 2009;46:4133–49.

[52] Rodigari D, Franchi A, Genna F, Crespi P, De Col R. A linear complementarity approach to the time integration of dynamic elastic-plastic structural problems. Meccanica 2019;54:1597–609.

[53] Cottle RW. Symmetric dual quadratic programs. Q Appl Math 1963;21:237–43.

[54] Kostreva MM. Cycling in linear complementarity problems. Math Program 1979;16:127–30.

[55] Lemke CE. Bimatrix equilibrium points and mathematical programming. Manage Sci 1965;11:681–9.

[56] Lloyd Smith D, Sahlit CL. Rigid plastic dynamics. Math. Program. methods Struct. Plast., Springer; 1990, p. 293–313.

[57] Lloyd Smith D, Sahlit CL. Dynamic response of pulse loaded structures as a linear complementarity problem. Eng Optim 1991;18:23–41.

[58] Murty KG, Yu F-T. Linear complementarity, linear and nonlinear programming. vol. 3.

Citeseer; 1988.

[59] Karlos V., Solomos G., Calculation of Blast Loads for Application to Structural Components, Technical Report, European Commission Joint Research Centre, Institute for the Protection and Security of the Citizen, 2013